

Electronic Supplementary Information

Revealing the Activity of $\text{Co}_3\text{Mo}_3\text{N}$ and $\text{Co}_3\text{Mo}_3\text{N}_{0.5}$ as Electrocatalysts for the Hydrogen Evolution Reaction

Youyi Sun,^a Lewen Wang^b, Olga Guselnikova^{c, d}, Oleg Semyonov,^c James Fraser^a, Yecheng Zhou,^{* b} Núria López,^e and Alexey Ganin ^{* a}

^a School of Chemistry, University of Glasgow, Glasgow, G12 8QQ, UK

^b School of Materials Science & Engineering, Sun Yat-Sen University, Guangzhou 510006 Guangdong, P. R. China.

^c Tomsk Polytechnic University, Tomsk Polytechnic University, Lenina Av. 30, 634050 Tomsk, Russian Federation

^d National Institute for Materials Science (NIMS), 1-1 Namiki, Tsukuba, Ibaraki 305-0044, Japan

^e Institute of Chemical Research of Catalonia, The Barcelona Institute of Science and Technology, Tarragona, Spain

Experimental Details

Synthesis of $\text{Co}_3\text{Mo}_3\text{N}$

Firstly, the oxide precursor was prepared by using the Pechini's method with some modifications.^{1,2} In a typical synthesis, 5.66 mmol $\text{Co}(\text{NO}_3)_2 \cdot 6\text{H}_2\text{O}$ (Alfa Aesar, ACS reagent, $\geq 99.0\%$), 0.81 mmol $(\text{NH}_4)_6\text{Mo}_7\text{O}_{24} \cdot 4\text{H}_2\text{O}$ (Sigma-Aldrich, ACS reagent, $\geq 99.0\%$) and 22.6 mmol citric acid monohydrate, $\text{C}_6\text{H}_8\text{O}_7 \cdot \text{H}_2\text{O}$ (Alfa Aesar, $\geq 99.5\%$) were added into a 150 ml pyrex beaker and fully dissolved in 80 ml deionised water on stirring at room temperature. The water was evaporated at 120 °C resulting in foam looking products. The foams were calcined within the same beaker in air in a box furnace at 500 °C for 12 hours to eliminate any traces of carbon. The calcined foam was reground to black powder and confirmed as carbon-free by elemental analysis. $\text{Co}_3\text{Mo}_3\text{N}$ was synthesised by nitridation of the oxide precursor prepared as described above. In a typical experiment, 200 mg of the oxide precursor were placed into a ceramic boat within a tube furnace. The samples were heated at 5 °C min^{-1} to 750 °C under the flow of H_2 (5 %) / N_2 gas (a flow rate of 10 mL min^{-1}). After 5 hours of reaction time the furnace was cooled naturally to the ambient temperature and the synthesised products were reground with a pestle and mortar.

Synthesis of $\text{Co}_3\text{Mo}_3\text{N}_{0.5}$

$\text{Co}_3\text{Mo}_3\text{N}_{0.5}$ samples were prepared following a modified procedure described elsewhere.³ In a typical experiment, 100 mg of $\text{Co}_3\text{Mo}_3\text{N}$ were placed into a ceramic boat which was placed into a tube furnace and then heated at 5 °C min^{-1} to 750 °C in a flow of 10 mL min^{-1} of H_2 (5 vol. %) / Ar gas mixture. After 2 hours of reaction time the furnace was cooled naturally to the ambient temperature.

Synthesis of $\text{Co}_3\text{Mo}_3\text{N}$ on Ni form

In a typical synthesis, 0.162 mmol of $(\text{NH}_4)_6\text{Mo}_7\text{O}_{24} \cdot 4\text{H}_2\text{O}$ (Sigma-Aldrich, ACS reagent, $\geq 99.0\%$) and 1.132 mmol $\text{Co}(\text{NO}_3)_2 \cdot 6\text{H}_2\text{O}$ (Alfa Aesar, ACS reagent, $\geq 99.0\%$) were dissolved in 20 mL of deionized water and stirred for 30 mins to get pink solution. This solution transferred with prepared Ni form into a 45 mL PTFE-liner together with a piece of Ni form (1×1 cm), cleaned in 1M HCl for 10 mins, followed by rinsing with deionized water. The liner was sealed in a stainless-steel Parr jacket and let to react at 140 °C for 16 h. After cooling to room temperature, the Ni form was taken out, washed with DI water, and dried overnight at 60 °C in air. The Ni form was placed into tube furnace and reacted at 750 °C with 5% H_2/N_2 gas for 5 h.

Electrochemical testing

Catalysts were deposited on to the surface of a glassy carbon electrode (surface area 0.071 cm²) by initially preparing the materials as inks. This involved sonicating a mixture consisting of 1 mL DMF (99.9 %, Sigma-Aldrich), 0.05 mL Nafion (5 wt. % in mixture of lower aliphatic alcohols and water, Sigma-Aldrich) and 8 mg of nitride for 1 hour. After this time, 0.010 mL (corresponding to sample loading of *ca.* 1.13 mg cm⁻² geometric) of the ink was drop cast on to the glassy carbon working electrode and allowed to dry naturally in air. Co₃Mo₃N on Ni-foam was clamped with a crocodile clip and inserted into the electrolyte solution. The sample loading (*ca.* 1.28 mg cm⁻² geometric) for Co₃Mo₃N on Ni foam was determined by difference in weight between pristine Ni foam and Co₃Mo₃N@Ni-foam measured on a balance with the precision of ±0.00001 g. For the control experiments, 20% Pt on carbon (Sigma-Aldrich) was dispersed as inks and then deposited on to the surface of a glassy carbon electrode (surface area 0.071 cm²). This involved sonicating a mixture consisting of 1 mL DMF (99.9 %, Sigma-Aldrich), 0.05 mL Nafion (5 wt. % in mixture of lower aliphatic alcohols and water, Aldrich) and 8 mg of 20% Pt/C for 1 hour. After this time, 0.010 mL (corresponding to sample loading of *ca.* 1.13 mg cm⁻² geometric) of the ink was drop cast on to the glassy carbon working electrode and allowed to dry naturally in air.

Carbon felt and 3 M Ag/AgCl were used as the counter and reference electrodes, respectively. Electrode potentials were converted to RHE scale by $E(\text{NHE}) = E(\text{Ag}/\text{AgCl}) + 0.209 \text{ V} + 0.059 \times \text{pH}$, and the ohmic resistances were compensated. Polarisation curves and Tafel slopes were obtained by linear sweep voltammetry with a scan rate of 5 mV s⁻¹. During measurements the cell was kept under continuous stirring to remove any bubbles formed on the working electrode surface. Nyquist plots were obtained between a frequency range of 200 kHz to 100 mHz.

The values of capacitive current was obtained through sweeping the applied potential at various scan rate (20, 40, 60, 80, 100, 120, 140 mV s⁻¹), and a small potential range (0.05 V to -0.05 V vs. Ag(AgCl)) was used to make sure the non-faradic region investigated in this case.

The samples for XPS spectroscopy measurements were prepared as follows. Co₃Mo₃N inks were drop-casted onto two separate glassy carbon electrodes as described above. Five LSV scans were ran at 100 mV s⁻¹ on the first electrode after which it was rinsed with distilled water, dried in Ar flow and the resulting sample was used for XPS analysis. 1000 cycles of LSV at 100 mV s⁻¹ we carried out on the second electrode followed by rinsing, drying, and isolating the sample. To minimize the presence of Nafion at the surface of the samples they were irradiated with MAGCIS gun (over variable time range 960 -1920 s), working in a cluster mode using argon ions with energy ion energy 8000 (eV), cluster size 75, and raster size 500 μm².

Gas chromatography was used to confirm the production of hydrogen using an Agilent GC 7890 A with a thermal conductivity detector (see Supporting information for a detailed procedure). The column used was a 30 metre-long 0.320 mm widebore HP-molesieve column (Agilent). The GC oven temperature was set to 27 °C and the carrier gas was Ar. The front inlet was set to 100 °C. The GC system was calibrated using certified standards of hydrogen at various concentrations (vol%) in Ar (CK Gas Products Limited, UK) before use. The Faradaic efficiency of $\text{Co}_3\text{Mo}_3\text{N}$ was experimentally measured using a single cell two-electrode set up, which involved the catalyst-deposited glassy carbon working electrode and carbon felt counter electrode attached to a silver wire immersed in 0.5 M H_2SO_4 . A known volume of electrolyte was removed to accurately determine the cell headspace. The cell was then sealed and degassed under argon for 30 minutes thus insuring an airtight system. Galvanostatic electrolysis was then performed with an applied current of -0.24 mA. At regular intervals, 25 μL samples of the headspace were directly injected into the GC. The expected volume percentages of hydrogen in the headspace was calculated by converting the charge passed to an expected number of moles of gas, and then taking the volume of 1 mole of an ideal gas at room temperature and pressure to be 22.4 litre.

Calculation details of turnover frequencies (TOF) calculations

As determined by N_2 gas adsorption (BET) measurements the surface area of $\text{Co}_3\text{Mo}_3\text{N}$ catalyst is 2 $\text{m}^2 \text{g}^{-1}$ which corresponds to $2 \cdot 10^{-3} \text{m}^2 \text{mg}^{-1}$.

The sample loading on the electrode is 0.08 mg which translates into surface area of the product on the electrode ($0.08 \text{mg} \times 2 \cdot 10^{-3} \text{m}^2 \text{mg}^{-1}$) = $1.6 \cdot 10^{-4} \text{m}^2$. However, we should keep in mind that only the half of the product is exposed to electrolyte as the other half is facing the electrode surface. Therefore, the total area is $0.8 \cdot 10^{-4} \text{m}^2 = 8 \cdot 10^{-5} \text{m}^2$.

To calculate the number of catalytic sites we need to recall that according to our DFT calculations the most stable surface of $\text{Co}_3\text{Mo}_3\text{N}$ is described by the (111)- supercell (Fig. S19) with the unit cell dimension of $a = 1557.061$ pm. The surface area of the unit cell is a rhombus with the area of

$$S = a^2 \sin 60^\circ = (\sqrt{3}/2) \times (1557.061 \text{ pm})^2 = 2.1 \cdot 10^6 \cdot \text{pm}^2 = 2.1 \cdot 10^6 \times 10^{-24} \text{m}^2 = 2.1 \cdot 10^{-18} \text{m}^2.$$

The total number of catalytic sites (H2-IN, Fig. S25) in the unit cell is four. The total number (N) of atoms corresponding to catalytic sites at the surface is:

$$N = 4 \text{ sites} \times (8 \cdot 10^{-5} \text{m}^2 / 2.1 \cdot 10^{-18} \text{m}^2) = 15.2 \cdot 10^{13} \text{ at} = 1.52 \cdot 10^{14} \text{ sites}.$$

To create 1 mole of H_2 , it is required for 2 moles of electrons to pass through the electrolyte. This will require the total amount of charge $C = 2 \times 96485$ A s, where 96485 is the Faraday constant.

At a given current density (j) and geometrical electrode area (S_{geo}) the amount of H_2 in moles (n_{H_2}) generated every second is $n_{\text{H}_2} = (j \times S_{\text{geo}} \times 1 \text{ mole}) / (2 \times 96485 \text{ A s})$

For example, the total number of moles of H_2 generated every second at the current density of 10 mA cm^{-2} on the electrode used in this work is:

$$n_{H_2} = (10 \cdot 10^{-3} \text{ A cm}^{-2} \times 0.072 \text{ cm}^2 \times 1 \text{ mole}) / (2 \times 96485 \text{ A s}) = 3.73 \cdot 10^{-9} \text{ mole s}^{-1}.$$

If every catalytic site creates a H₂ molecule upon electrolysis, the turnover frequency can be calculated using the equation:

$$\text{TOF} = (j S_{\text{geo}} N_A) / (F n N),$$

where j is the current density, S_{geo} is the geometrical surface area of the electrode, N_A is Avogadro number, F is Faraday constant, n number of electrons transfer for creating one H₂ molecule, N is the number of catalytic sites.

At the current density of 10 mA / cm² the TOF for H₂ molecules on each site will be:

$$\text{TOF} = (10 \cdot 10^{-3} \text{ A cm}^{-2} \times 0.071 \text{ cm}^2 \times 6.023 \cdot 10^{23} \text{ molecule mol}^{-1}) / (96485 \text{ A s mol}^{-1} \times 2 \times 1.52 \cdot 10^{14} \text{ at.}) = (42.76 \cdot 10^{19} \text{ molecule} / 28.94 \cdot 10^{18} \text{ s site}) = 14.7 \text{ molecule site}^{-1} \text{ s}^{-1}$$

Calculation details for surface energies and chemical potentials

The surface energy was calculated using the equation $\gamma = E(\text{surface model}) - \sum_i n_i (E_i + \mu)$, where E_i and μ are the energy and chemical potential of element i . E_i was calculated based on the most stable phase of element i , is calculate $E_i = E(\text{unit cell}) / N(\text{number of atoms in the unit cell})$. The chemical potentials of these elements are determined by:

$$3\mu_{Co} + 3\mu_{Mo} + \mu_N = E(Co_3Mo_3N) - \sum_i n_i (E_i) = -0.643 \text{ eV} \quad (1)$$

To avoid the formation of MoN, $E(MoN) - (E_{Mo} + E_N) - (\mu_{Mo} - \mu_N) > 0$ we get

$$\mu_{Mo} + \mu_N < E(MoN) - \sum_i n_i (E_i) = -0.491 \text{ eV} \quad (2)$$

For the same reason, we have

$$2\mu_{Co} + \mu_N < E(Co_2N) - \sum_i n_i (E_i) = -0.799 \text{ eV} \quad (3) \quad (\text{to avoid the formation of CoN})$$

$$3\mu_{Co} + \mu_{Mo} < E(Co_3Mo) - \sum_i n_i (E_i) = -0.091 \text{ eV} \quad (4) \quad (\text{to avoid the formation of Co}_3\text{Mo})$$

$$2\mu_{Co} + 4\mu_{Mo} + \mu_N < E(Co_2Mo_4N) - \sum_i n_i (E_i) = -3.840 \text{ eV} \quad (5) \quad (\text{to avoid the formation of Co}_3\text{Mo}_4\text{N})$$

$$\mu_{Co} < 0 \text{ and } \mu_{Mo} < 0 \quad (6) \quad (\text{to avoid the formation of Co and Mo metals})$$

$$\text{eq(1)} - \text{eq(2)}: 3\mu_{Co} + 2\mu_{Mo} > -0.152 \quad (7)$$

$$\text{eq(1)} - \text{eq(5)}: \mu_{Co} - \mu_{Mo} > 3.197 \text{ eV} \quad (8)$$

$$\text{eq(7)} + 2 \text{ eq(8)}: 4\mu_{Co} > 5.751 \text{ eV},$$

which contradict with eq(6). This is because $\text{Co}_3\text{Mo}_3\text{NC}$ will decomposes into $\text{Co}_2\text{Mo}_4\text{N}$, Co_3Mo and MoN based on their energies, which also indicated in the Materials-Project (<https://materialsproject.org/materials/mp-22166/>). But the decomposition may require larger activation energies. We here remove the $\text{Co}_2\text{Mo}_4\text{N}$ phase. From eq(4) and eq(6), we have $-0.030 < \mu_{\text{Co}} < 0$; and $-0.091 < \mu_{\text{Mo}} < 0$. As lower μ_{Co} has more opportunity to form $\text{Co}_2\text{Mo}_4\text{N}$, we take $\mu_{\text{Co}} = 0$ eV. From eq(7), we have $-0.076 < \mu_{\text{Mo}} < 0$. For computational convenience, we take $\mu_{\text{Mo}} = -0.060$ eV. We get $\mu_{\text{N}} = -0.461$ eV.

The zero-point vibration energy (ZPE) was performed by the frequency calculation of VASP, which is $E(\text{ZPE}) = \sum_i \hbar v_i$, where v_i is the frequency of normal mode i .

The gas entropy contribution of free energy (TS) was obtained from national institute of standards and Technology (NIST). As the entropy of adsorbed H was very small, we set it to zero. ZPE of different adsorbed H were calculated from which we found that the ZPE of different adsorbed H are nearly constant, which is about 0.187 eV. Hence, the ZPE energy of all adsorbed H are set to 0.187 eV in this work.

		$(C_p - S) * T$ (eV)	ZPE (eV)	mean ZPE (eV)
Gas	$\text{H}_2(\text{gas})$	-0.316	0.282	
Adsorbed H	H2	0	0.196	0.187
	B1-H1	0	0.178	
	H1	0	0.191	
	T1	0	0.184	

Table S1. Electrochemical properties of previously reported nitrides for the HER in acidic media

Reported material description	η , mV at 10 mA cm ⁻² (acidic media)	Tafel slope, mV dec ⁻¹	ECSA, mF cm ⁻²	Catalyst loading, mg/cm ²	Ref.
NiMoN _x /C nanosheet	220 (0.1M HClO ₄) @5 mA cm ⁻²	36	N/A	0.25	4
Co _{0.6} Mo _{1.4} N ₂	200 (0.1M HClO ₄)	N/A	N/A	0.24	5
Co ₃ Mo ₃ N	>400 (0.1M HClO ₄) @5 mA cm ⁻²	N/A	N/A	N/A	5
W-doped MoN	129 (0.5M H ₂ SO ₄)	59	N/A	0.4	6
Pt-TiN NTAs	71 (0.5M H ₂ SO ₄)	46.4	67.9	N/A	7
Ru-VN	134 (0.5M H ₂ SO ₄)	35	N/A	N/A	8
Co/WN	208 (0.5M H ₂ SO ₄)	92	308	N/A	9
P-MoP/Mo ₂ N	89 (0.5M H ₂ SO ₄)	53	N/A	N/A	10
MoS ₂ /Mo ₃ N ₂ hybrid	196 (0.5M H ₂ SO ₄)	79	14.15	N/A	11
Co ₃ Mo ₃ N	108±8 (0.5M H ₂ SO ₄)	80±8	17.8±6	1.13	This work
Co ₃ Mo ₃ N _{0.5}	117±12 (0.5M H ₂ SO ₄)	79±6	16.9±4	1.13	This work

Table S2 Structural parameters for the Rietveld refinement of the PXRD data collected on $\text{Co}_3\text{Mo}_3\text{N}$ powder sample using structural model based on $\eta\text{-W}_3\text{Fe}_3\text{C}$ structure-type (Space group: $Fd\text{-}3mz$) at ambient temperature. Estimated errors in the last digits are given in parentheses. The value of the lattice constant $a = 1101.39 \pm 0.03$ pm. (Literature: $a = 1102.09$ pm prepared in $\text{H}_2(10\%)/\text{N}_2$; 1102.70 pm and 1103.83 pm prepared by ammonolysis of metal oxides in NH_3).^{2,5,12,13}

	Site	x/a	y/b	z/c	Occupancy	B_{iso} (pm^2)
Mo	48f	0.3250(1)	0.125	0.125	1.0	47(4)
Co1	32e	0.2922(1)	0.2922(1)	0.2922(1)	1.0	71(9)
Co2	16d	0.5	0.5	0.5	1.0	70(13)
N	16c	0	0	0	1.0	38

Table S3 Structural parameters for the Rietveld refinement of the PXRD data collected on $\text{Co}_3\text{Mo}_3\text{N}_{0.5}$ powder sample using structural model based on $\eta\text{-Co}_6\text{Mo}_6\text{C}$ structure-type (Space group: $Fd\text{-}3mz$) at ambient temperature. Estimated errors in the last digits are given in parentheses. The value of the lattice constant $a = 1088.10 \pm 0.01$ pm. (Literature: $a = 1088.24$ pm).³

	Site	x/a	y/b	z/c	Occupancy	B_{iso} (pm^2)
Mo	48f	0.3216(1)	0.125	0.125	1.0	70(5)
Co1	32e	0.2936(1)	0.2936(1)	0.2936(1)	1.0	78(13)
Co2	16d	0.5	0.5	0.5	1.0	70(18)
N	8a	0.125	0.125	0.125	1.0	38

Table S4: Results of the EDXS analysis collected in multiple random spots across samples of $\text{Co}_3\text{Mo}_3\text{N}$, $\text{Co}_3\text{Mo}_3\text{N}_{0.5}$ and $\text{Fe}_3\text{Mo}_3\text{N}$. The errors are calculated as additive of the standard deviation of the averages from 6 spots and the instrumental error of 0.81 %. Due to the semi-qualitative nature of the detection of light elements by EDXS the N-content was excluded from the calculations.

Element	$\text{Co}_3\text{Mo}_3\text{N}$ at. %		$\text{Co}_3\text{Mo}_3\text{N}_{0.5}$ at. %		$\text{Fe}_3\text{Mo}_3\text{N}$ at. %	
	Co	Mo	Co	Mo	Fe	Mo
Experiment	45.56 \pm 1.05	54.43 \pm 1.05	45.94 \pm 0.55	54.06 \pm 0.55	45.91 \pm 0.45	54.09 \pm 0.45
Theory	50	50	50	50	50	50

Table S5. The positions of Mo 3d peaks before and after 1000 scans in 0.5 M H₂SO₄.

Sample	Peak position					
	Mo ⁰ 3d _{5/2}	Mo ⁰ 3d _{3/2}	Mo-N 3d _{5/2}	Mo-N 3d _{3/2}	Mo-O 3d _{5/2}	Mo-O 3d _{3/2}
Co₃Mo₃N before	227.7	230.8	228.5	231.8	232.4	235.4
Co₃Mo₃N after	227.9	231.1	228.7	232.0	232.6	235.6

Table S6. The areas of Mo 3d peaks before and after 1000 scans in 0.5 M H₂SO₄.

Sample	Area					
	Mo ⁰ 3d _{5/2}	Mo ⁰ 3d _{3/2}	Mo-N 3d _{5/2}	Mo-N 3d _{3/2}	Mo-O 3d _{5/2}	Mo-O 3d _{3/2}
Co₃Mo₃N Before	119170	81000	77438	53462	18624	12093
Co₃Mo₃N after	104454	68719	78914	54483	12585	8689

Table S7. Full width at half maximum (FWHM) of Mo 3d before and after 1000 scans in 0.5 M H₂SO₄.

Sample	FWHM					
	Mo ⁰ 3d _{5/2}	Mo ⁰ 3d _{3/2}	Mo-N 3d _{5/2}	Mo-N 3d _{3/2}	Mo-O 3d _{5/2}	Mo-O 3d _{3/2}
Co₃Mo₃N Before electro	0.86	1.10	2.68	2.68	1.9	1.9
Co₃Mo₃N After electro	0.86	1.10	1.98	1.98	1.67	1.67

Table S8. The positions of Co 2p peaks before and after 1000 scans in 0.5 M H₂SO₄.

Sample	Peak position									
	Co ⁰ 2p _{3/2}	Co ⁰ 2p _{1/2}	Co ⁰ loss features + Co-N (2p _{3/2})	Co-N (2p _{1/2})	Co-O (2p _{3/2})	Co-O (2p _{1/2})	Co-N satellite (2p _{3/2})	Co-N satellite (2p _{1/2})	Co-O satellite (2p _{3/2})	Co-O satellite (2p _{1/2})
Co₃Mo₃N Before electro	778.1	792.8	779.3	794.0	781.3	796.9	784.2	800.0	787.9	803.6
Co₃Mo₃N After electro	778.4	793.1	779.3	794.0	781.3	797.0	784.3	800.0	787.8	803.6

Table S9. The areas of Co 2p peaks before and after 1000 scans in 0.5 M H₂SO₄.

Sample	Area									
	Co ⁰ 2p _{3/2}	Co ⁰ 2p _{1/2}	Co ⁰ loss features + Co-N (2p _{3/2})	Co-N (2p _{1/2})	Co-O (2p _{3/2})	Co-O (2p _{1/2})	Co-N satellite (2p _{3/2})	Co-N satellite (2p _{1/2})	Co-O satellite (2p _{3/2})	Co-O satellite (2p _{1/2})
Co₃Mo₃N Before electro	78339	29954	72359	37518	67965	35715	25134	13025	25212	13065
Co₃Mo₃N After electro	72837	28535	76918	40080	40376	20924	26079	13515	35525	17964

Table S10. The areas of Co 2p peaks before and after 1000 scans in 0.5 M H₂SO₄.

Sample	FWHM									
	Co ⁰ 2p _{3/2}	Co ⁰ 2p _{1/2}	Co ⁰ loss features + Co-N (2p _{3/2})	Co-N (2p _{1/2})	Co-O (2p _{3/2})	Co-O (2p _{1/2})	Co-N satellite (2p _{3/2})	Co-N satellite (2p _{1/2})	Co-O satellite (2p _{3/2})	Co-O satellite (2p _{1/2})
Co₃Mo₃ N Before electro	1.00	1.00	3.5	3.5	3.5	3.5	3.38	3.38	3.5	3.5
Co₃Mo₃ N After electro	1.01	1.01	3.22	3.22	3.5	3.5	3.5	3.5	3.5	3.5

Table S11. The positions of Mo 3p peaks before and after 1000 scans in 0.5 M H₂SO₄.

Sample	Peak position				
	Mo ⁰ + Mo-N 3p _{3/2}	Mo ⁰ + Mo-N 3p _{1/2}	N 1s	Mo-O 3p _{3/2}	Mo-O 3p _{1/2}
Co₃Mo₃N Before electro	393.8	411.4	397.0	398.0	415.1
Co₃Mo₃N After electro	394.1	411.7	397.0	398.2	415.0

Table S12. The areas of Mo 3p peaks before and after 1000 scans in 0.5 M H₂SO₄.

Sample	Area				
	Mo ⁰ + Mo-N 3p _{3/2}	Mo ⁰ + Mo-N 3p _{1/2}	N 1s	Mo-O 3p _{3/2}	Mo-O 3p _{1/2}
Co₃Mo₃N Before electro	145893	74666	8243	44012	22133
Co₃Mo₃N After electro	127039	65017	7594	38389	19359

Table S13. Full width at half maximum (FWHM) of Mo 3p before and after 1000 scans in 0.5 M H₂SO₄.

Sample	FWHM				
	Mo ⁰ + Mo-N 3p _{3/2}	Mo ⁰ + Mo-N 3p _{1/2}	N 1s	Mo-O 3p _{3/2}	Mo-O 3p _{1/2}
Co₃Mo₃N Before electro	3.24	3.24	2.09	3.5	3.5
Co₃Mo₃N After electro	3.02	3.02	1.88	3.0	3.0

Table S14. Surface energies (γ) of $\text{Co}_3\text{Mo}_3\text{N}$ (111) surfaces. N_{Co} , N_{Mo} and N_{N} number of atoms within the block. These surface structures are presented in Figure S12.

Surface index	N_{Co}	N_{Mo}	N_{N}	γ (J m^{-2})
Surface-0	100	120	44	1.927
Surface-1	112	120	44	3.013
Surface-2	112	132	44	3.421
Surface-3	116	132	44	3.419
Surface-4	128	132	48	3.096
Surface-5	132	132	48	3.026
Surface-6	132	144	48	2.739
Surface-7	144	144	48	3.133
Surface-8	144	156	48	3.337
Surface-9	148	156	60	2.603
Surface-10	148	168	60	2.008

Table S15. Possible adsorption sites and corresponding ΔG_H adsorption energies at pH = 0 in $\text{Co}_3\text{Mo}_3\text{N}$. Site notations are shown in Figure S18-S19. The initial adsorption site corresponds to the starting position of the H in the model. The final location corresponds to the final position of H upon optimisation.

Initial adsorption	Final H location*	ΔG_{Hads}(eV)
B1	H1	-0.21
B2	H1	-0.40
B3	H3	-0.29
B4	B4	-0.20
B5	H2-OUT	0.03
B6	H3	-0.25
H1	H1	-0.28
H2	H2-IN	0.49
H3	H3	-0.46
T1	T1	0.36
T2	B1	-0.22
T3	H3	-0.25
T4	H3	-0.45

Table S16. The final adsorption sites and adsorption energy in $\text{Co}_3\text{Mo}_3\text{N}$ after the optimisation of the model. The site notations are shown in Figure S18 and Figure S19.

Material	$\text{Co}_3\text{Mo}_3\text{N}$
Adsorption	$\Delta G_{\text{Hads}}(\text{eV})$
B1	-0.22
B4	-0.20
H1	-0.40
H2-IN	0.49
H3	-0.46
T1	0.36
H2-OUT	0.03

Table S17. The optimal sites and corresponding ΔG_H adsorption energies at pH = 0 in $\text{Co}_3\text{Mo}_3\text{N}$ for simultaneous adsorption on two sites. The site notations are identical to those shown in Figure S18 and Figure S19. $\Delta G_{\text{Hads}} = G_{\text{Hads}}(1,2) - G_{\text{Hads}}(1) - 1/2G_{\text{H}_2}$, is the H adsorption energy of site 2. $G_{\text{Hads}}(1,2)$ is the Gibbs free energy of the model that two sites (site 1 and site 2) are adsorbed. $G_{\text{Hads}}(1)$ is the Gibbs free energy of the model that site 1 is adsorbed.

Adsorption site 1	Adsorption site 2	Adsorption sites after relaxation of the model	$\Delta G_{\text{Hads}}(\text{eV})$
H1	B5	H1 / T2	0.48
H3	B5	H3 / T2	0.29
H3	H2	H1 / H2-IN	0.29
H1	H2	H1 / H2-OUT	0.27

Table S18. The optimal sites and corresponding ΔG_H adsorption energies at pH = 0 in $\text{Co}_3\text{Mo}_3\text{N}$ for simultaneous adsorption on three sites. The site notations are identical to those shown in Figure S18 and Figure S19. $\Delta G_{\text{Hads}} = G_{\text{Hads}}(1,2,3) - G_{\text{Hads}}(1,2) - 1/2G_{\text{H}_2}$, is the H adsorption energy of site 3. $G_{\text{Hads}}(1,2,3)$ is the Gibbs free energy of the model that three sites (site 1, site 2 and site 3) are adsorbed. $G_{\text{Hads}}(1,2)$ is the Gibbs free energy of the model that two sites (site 1 and site 2) are adsorbed.

Adsorption site 1	Adsorption site 2	Adsorption site 3	Adsorption sites after relaxation of the model	$\Delta G_{\text{Hads}}(\text{eV})$
H1	H3	B5	H1 / H3 / T2	0.34
H1	H3	H2	H1 / H3 / H2-IN	0.13

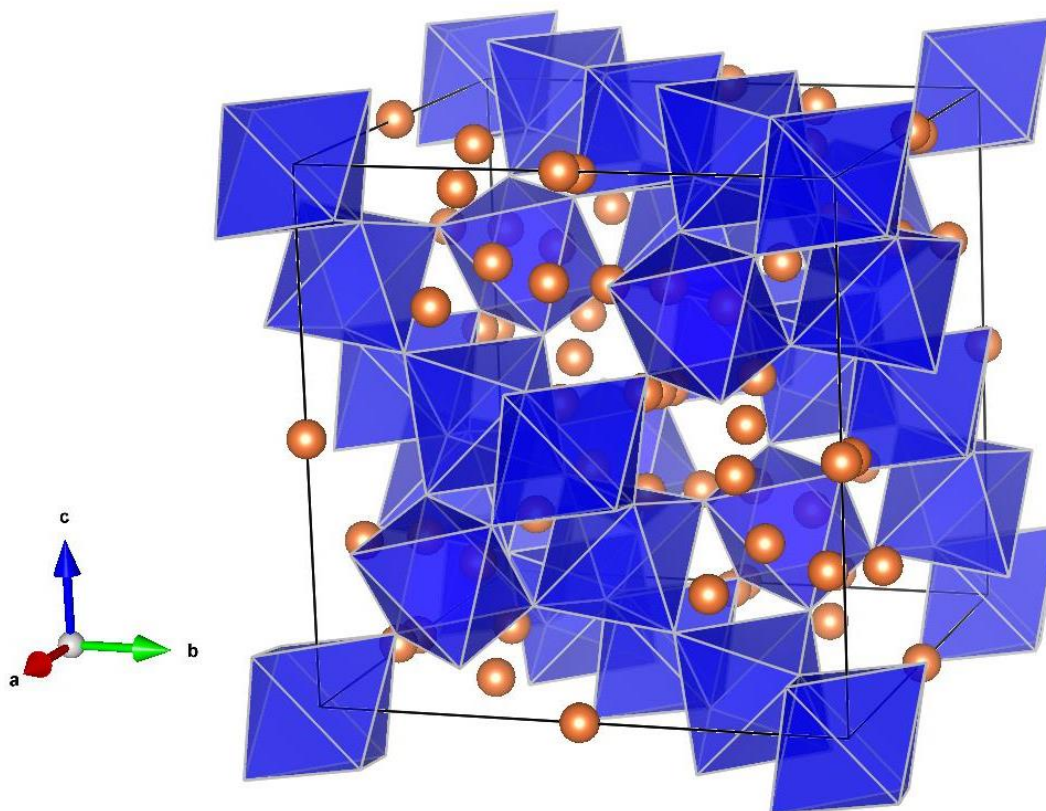


Figure S1. Crystal structure of $\text{Co}_3\text{Mo}_3\text{N}$ showing the network of corner sharing Mo_6N -octahedra (blue). Mo and N atoms are omitted for clarity while Co-atoms are shown as orange spheres.

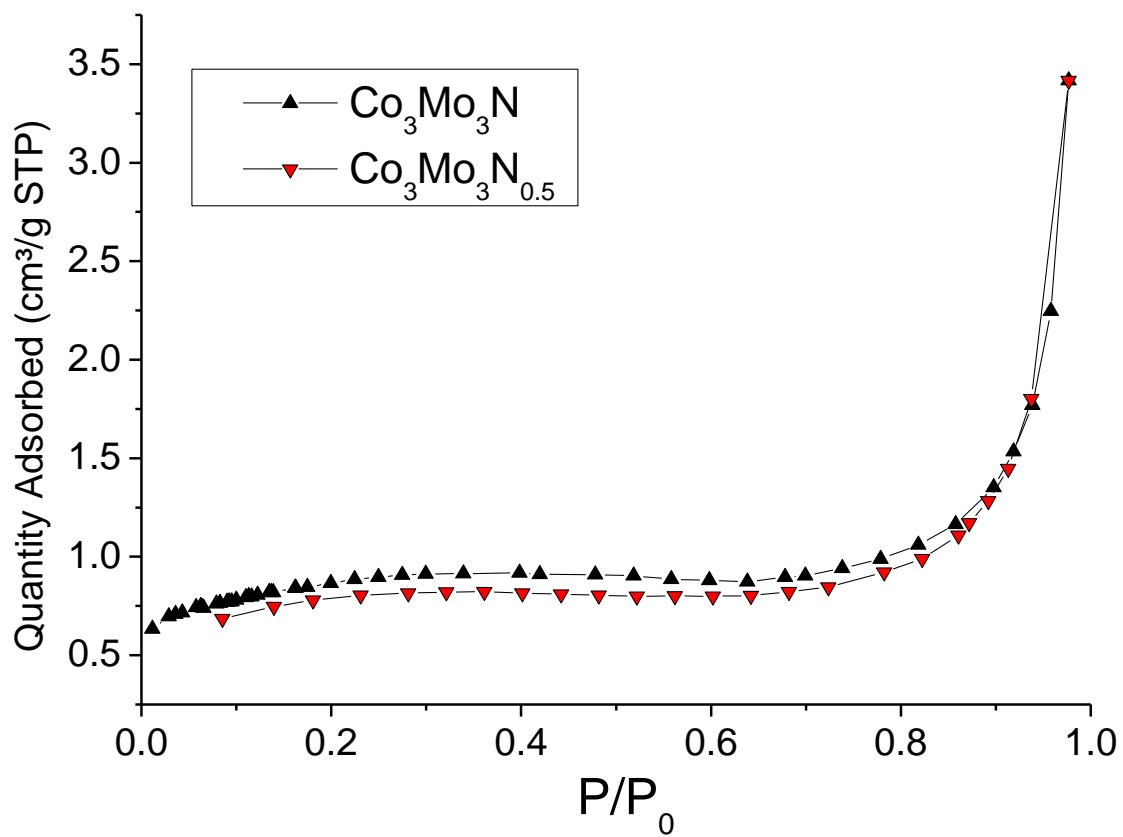


Figure S2. The nitrogen adsorption isotherm recorded on $\text{Co}_3\text{Mo}_3\text{N}$ and $\text{Co}_3\text{Mo}_3\text{N}_{0.5}$. The adsorption isotherms are generally consistent with the Type II isotherms.

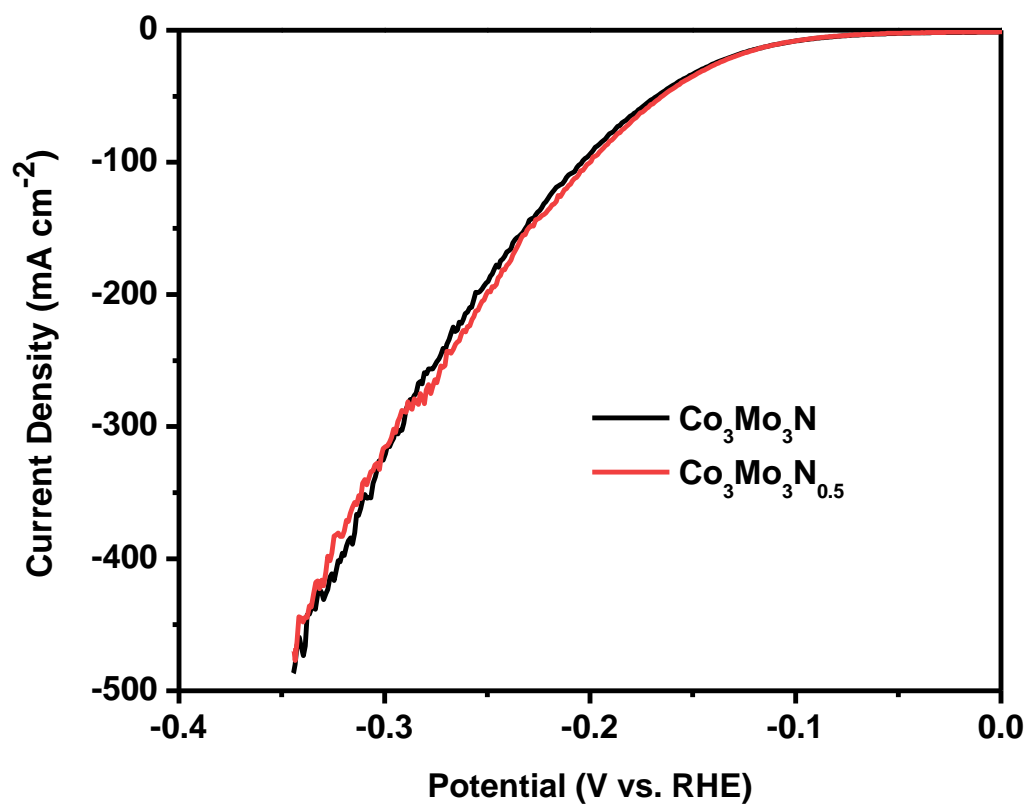


Figure S3. Comparison of the current densities achieved by $\text{Co}_3\text{Mo}_3\text{N}$ and $\text{Co}_3\text{Mo}_3\text{N}_{0.5}$ and obtained by linear sweep voltammetry at a scan rate of 5 mV s^{-1} .

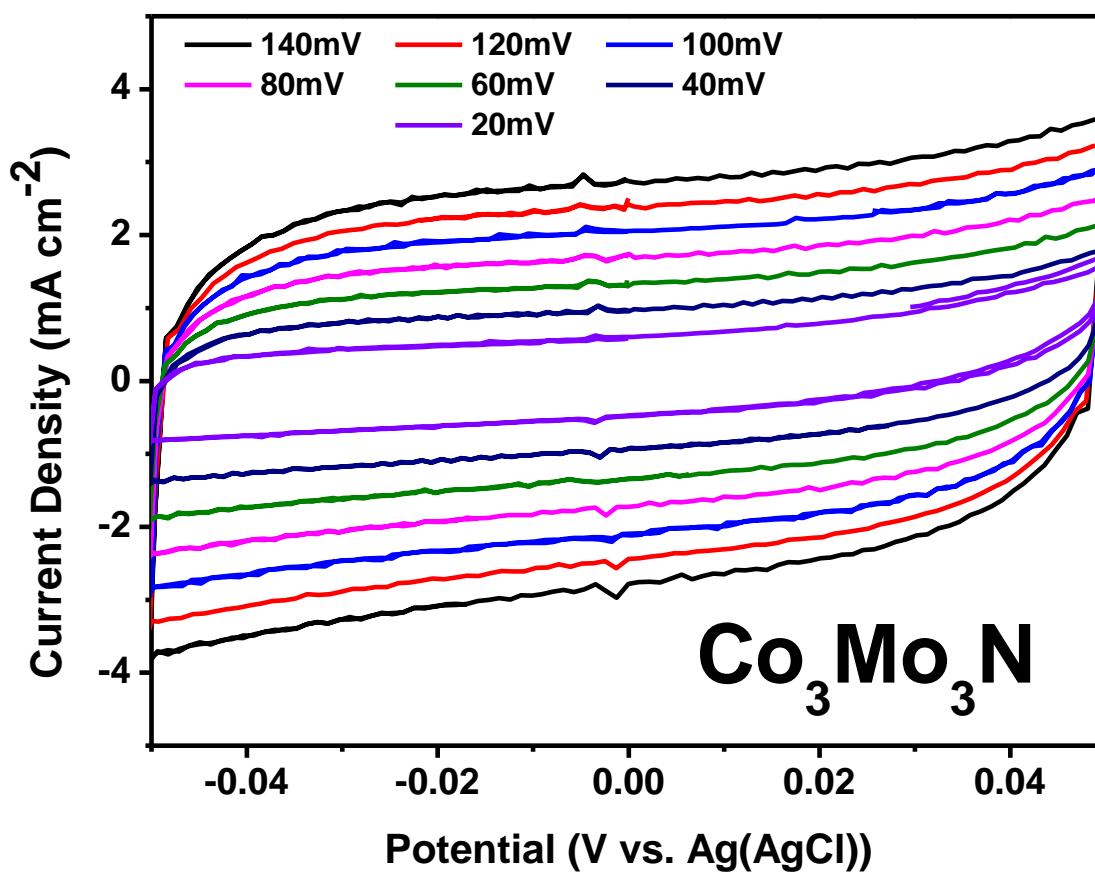


Figure S4. Cyclic voltammograms of $\text{Co}_3\text{Mo}_3\text{N}$ with different scan rates from 20 to 140 mV s^{-1} in the potential range of -0.05 to 0.05 V (vs Ag(AgCl)) in 0.5 M H_2SO_4 .

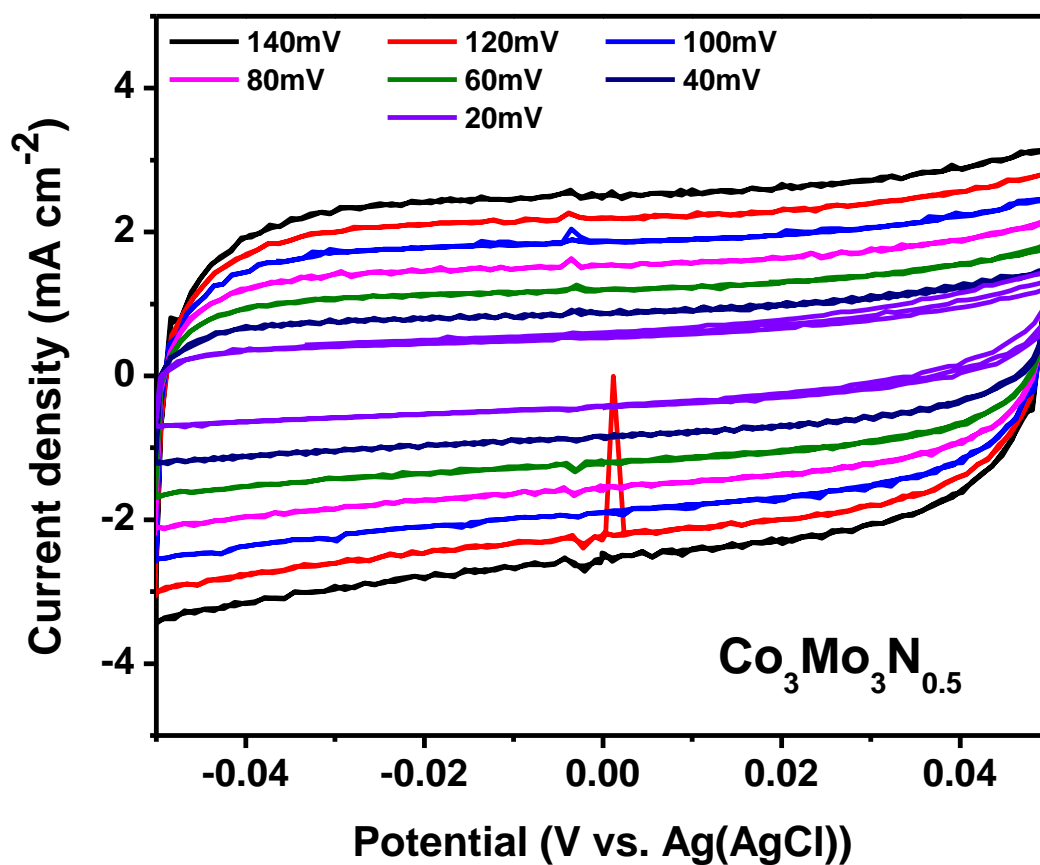


Figure S5. Cyclic voltammograms of $\text{Co}_3\text{Mo}_3\text{N}_{0.5}$ with different scan rates from 20 to 140 mV s^{-1} in the potential range of -0.05 to 0.05 V (vs Ag(AgCl)) in 0.5 M H_2SO_4 .

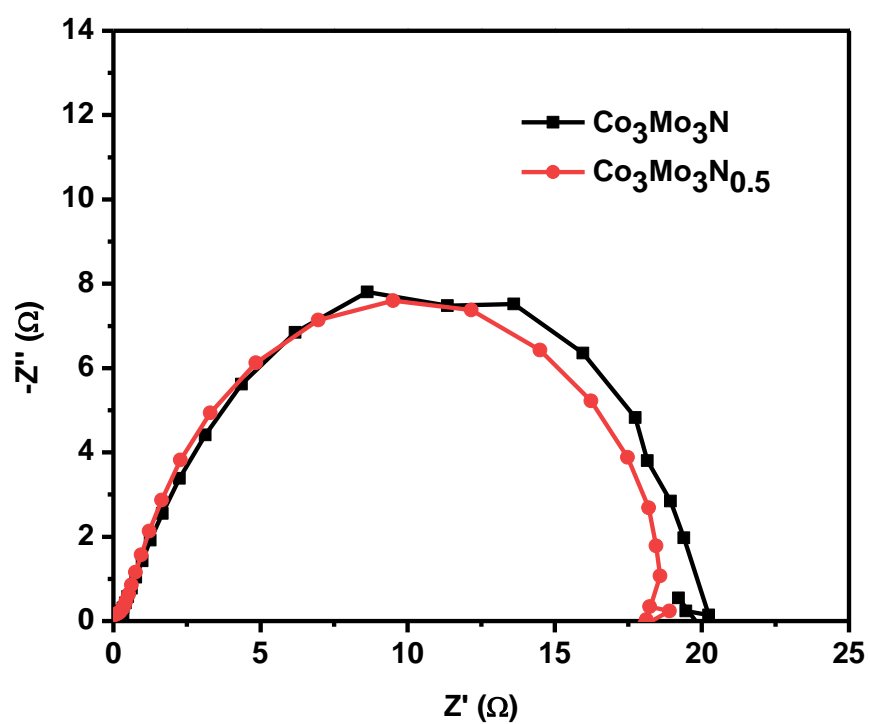


Figure S6. Electrochemical impedance spectroscopy (EIS) presented in form of Nyquist plots in a frequency range from 200 kHz to 100 mHz.

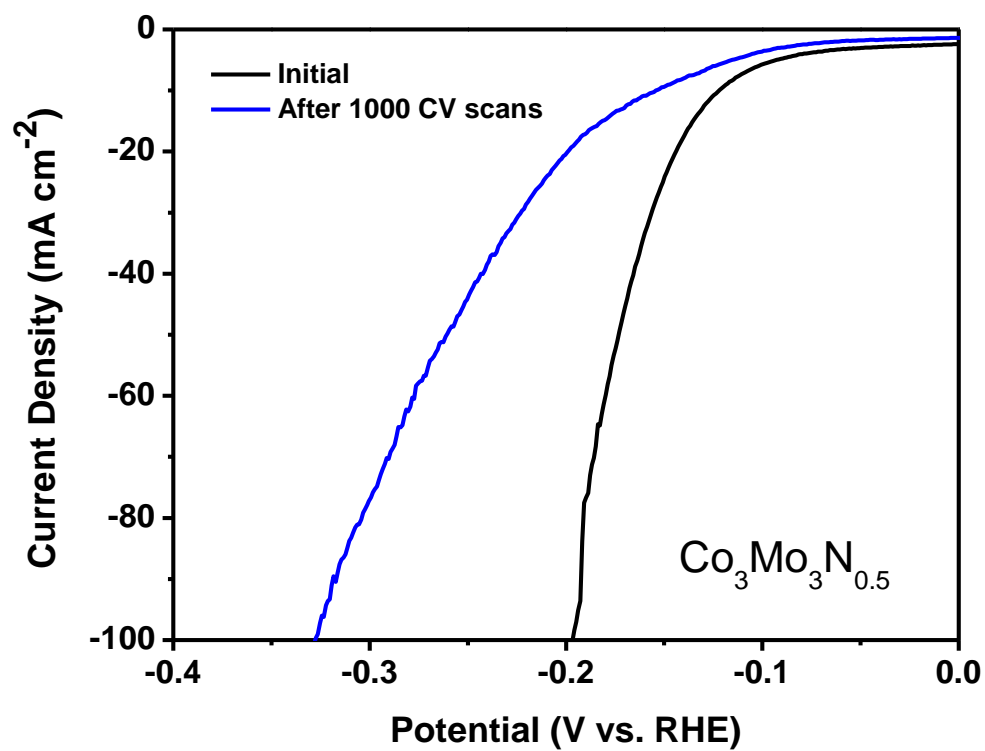


Figure S7: Comparison of the current densities achieved by Co₃Mo₃N_{0.5} catalyst in 0.5 M H₂SO₄ before and after 1000 cycles at the scan rate of 100mV s⁻¹.

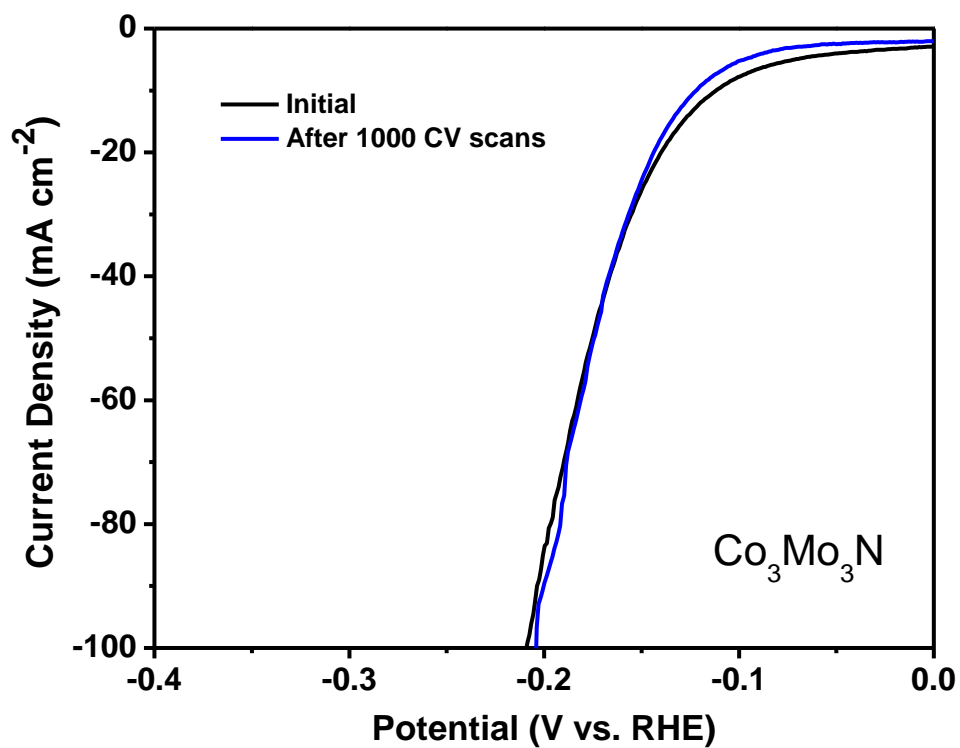


Figure S8: Comparison of the current densities achieved by $\text{Co}_3\text{Mo}_3\text{N}$ catalyst in 0.5 M H_2SO_4 before and after 1000 cycles at the scan rate of 100mV s^{-1} .

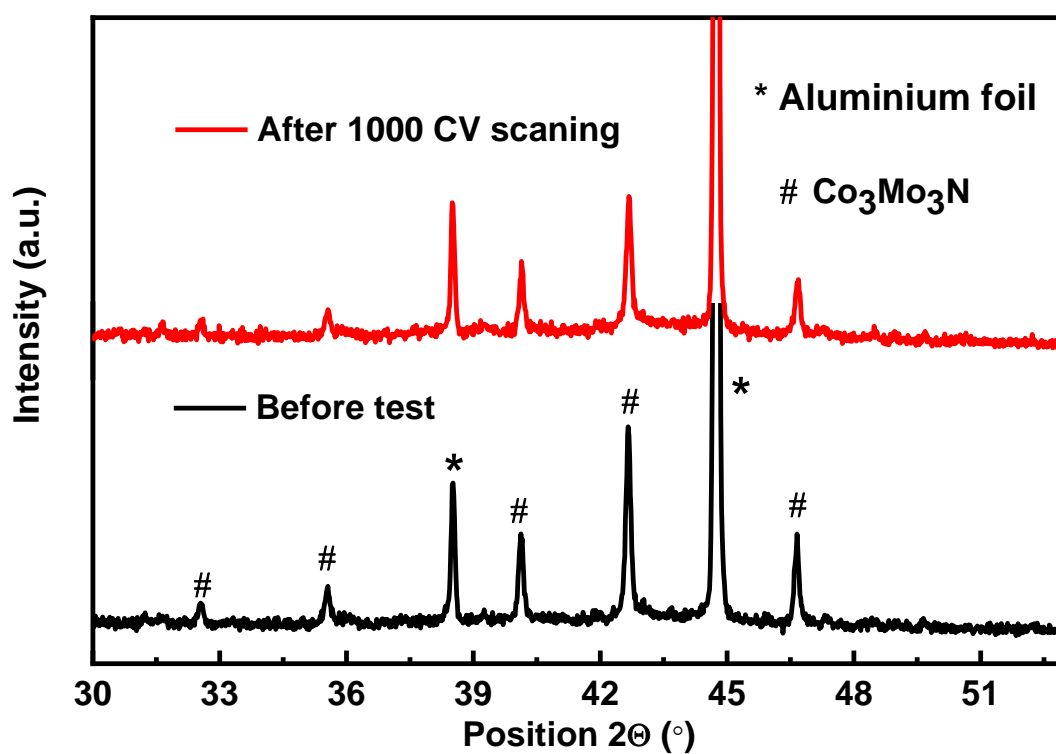


Figure S9. Comparison of PXRD patterns recorded on $\text{Co}_3\text{Mo}_3\text{N}$ before and after 1000 scans at the scan rate of 100 mV s^{-1} in $0.5\text{M H}_2\text{SO}_4$.

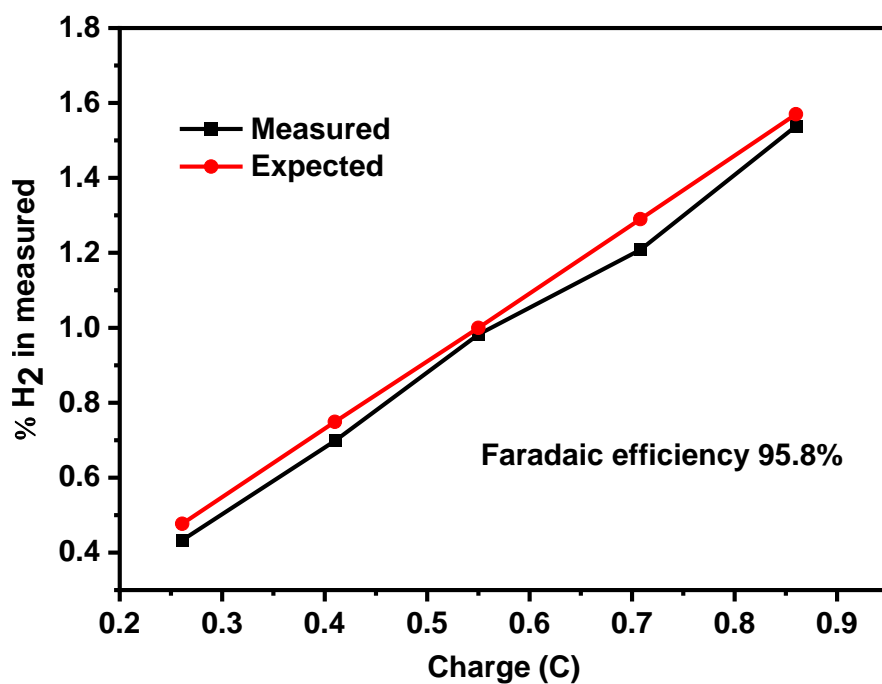


Figure S10. A representative trace of the proportion of H₂ (in vol. %) in the single-cell headspace during the electrolysis of Co₃Mo₃N at a constant current of 108 mA in 0.5 M H₂SO₄. Black squares show the proportion of H₂ (in vol. %) in the cell headspace determined using gas chromatography. The expected proportion of H₂ (in vol %) in the headspace was calculated from the charge passed.

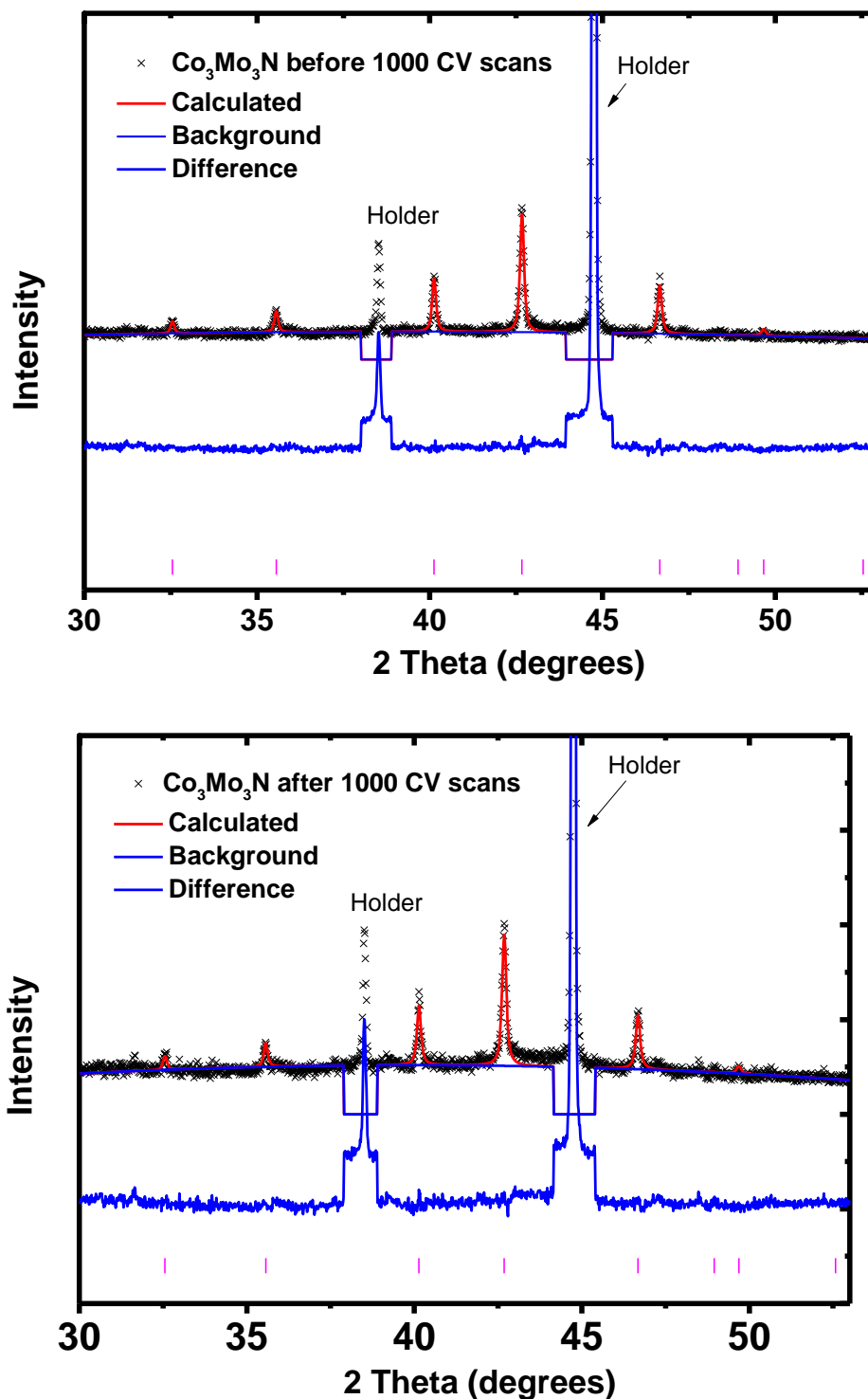


Figure S11. Rietveld refinement of PXRD data for $\text{Co}_3\text{Mo}_3\text{N}$ (collected directly on the electrode before and after 1000 cycles) showed in Fig. S9. The refinement was carried out using a structure model based on $\text{Co}_3\text{Mo}_3\text{N}$ structure (Space group: $Fd-3mz$). Measured data are shown as crosses; the calculated profile is shown by a solid red line. The difference profile is shown as blue line along the bottom of the plot. Vertical bars represent the reflection positions for the phase. The peaks associated with Al foil from the holder were excluded from the refinement.

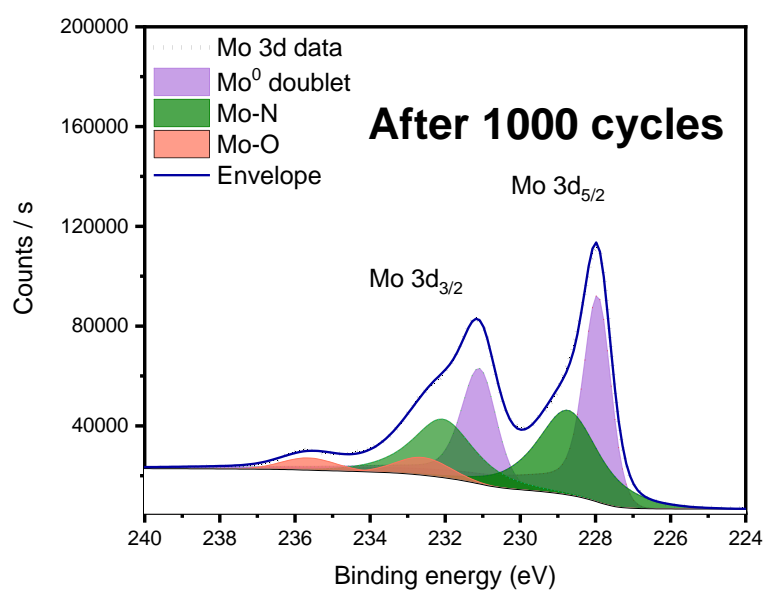
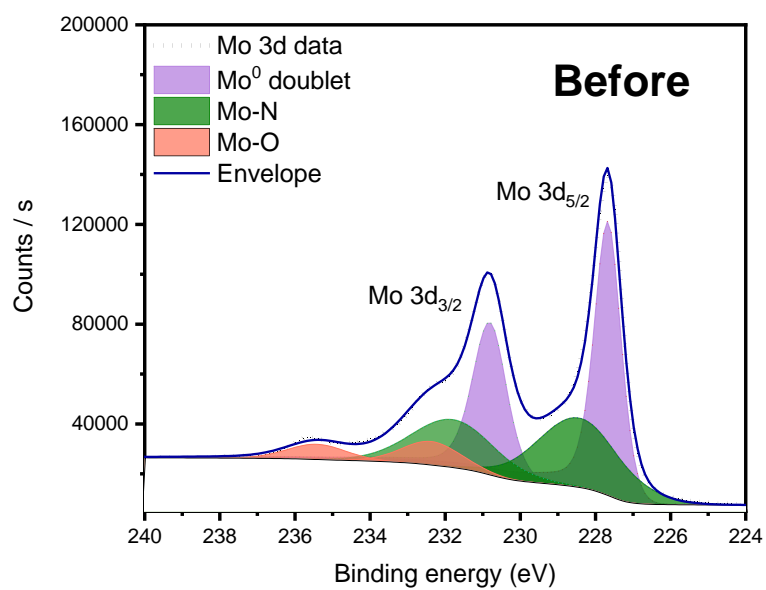


Figure S12. Experimental and deconvoluted high resolution Mo 3d XPS spectra before and after 1000 cycles in 0.5 M H₂SO₄.

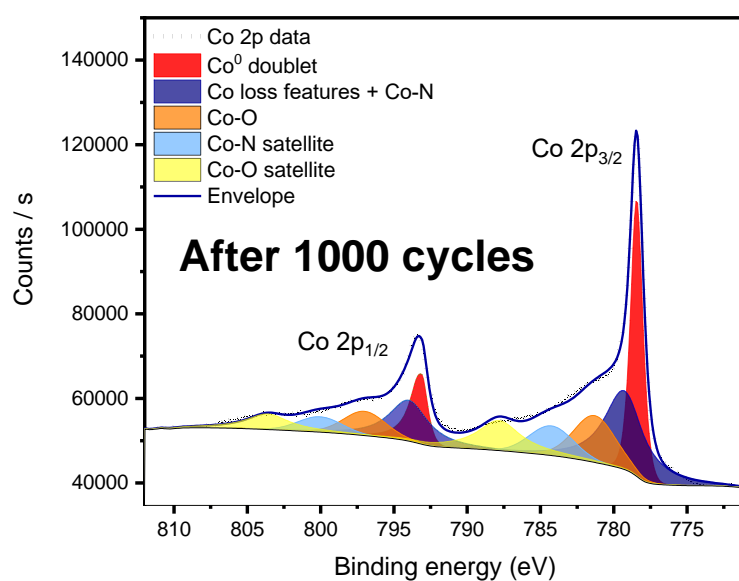
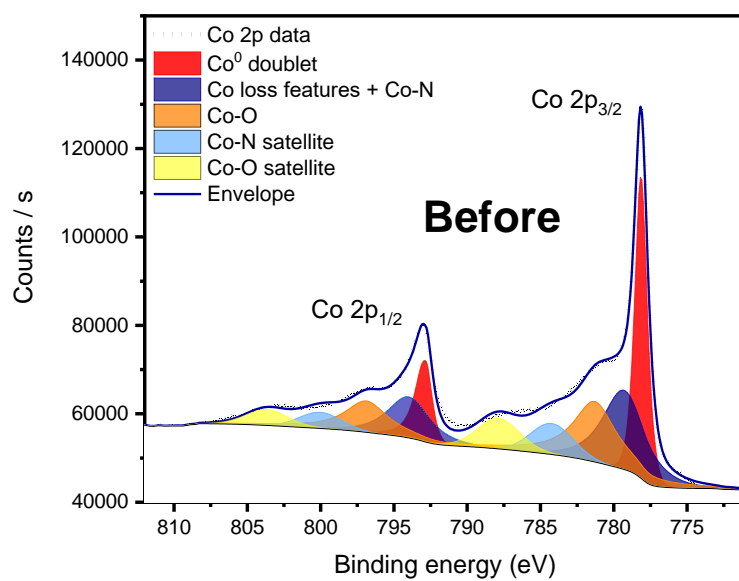


Figure S13. Experimental and deconvoluted high resolution Co 2p XPS spectra before and after 1000 cycles in 0.5 M H₂SO₄.

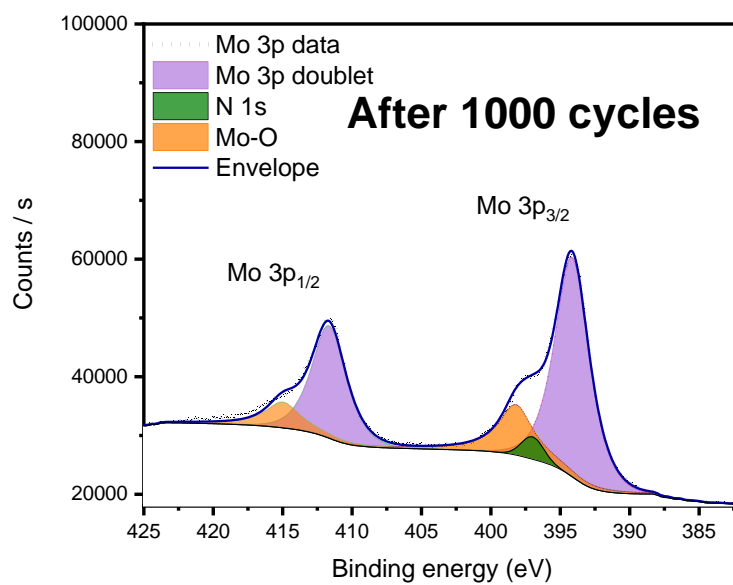
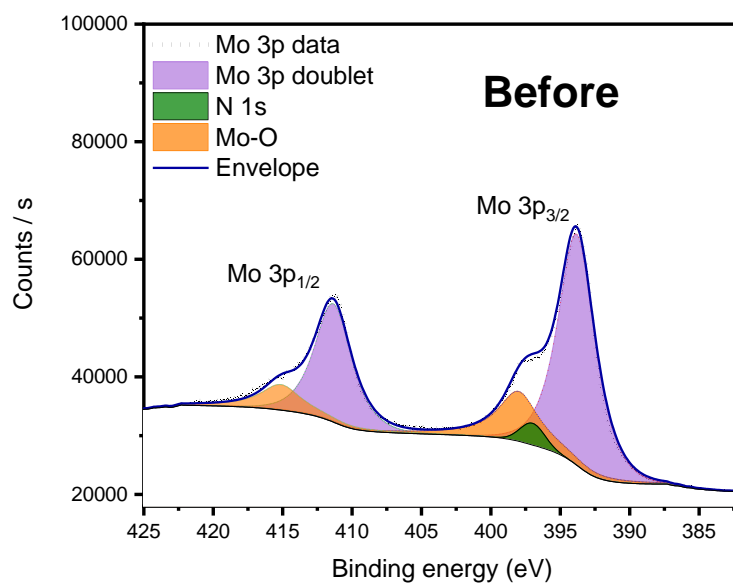


Figure S14. Experimental and deconvoluted high resolution Mo 3p and N 1s XPS spectra before and after 1000 cycles in 0.5 M H₂SO₄.

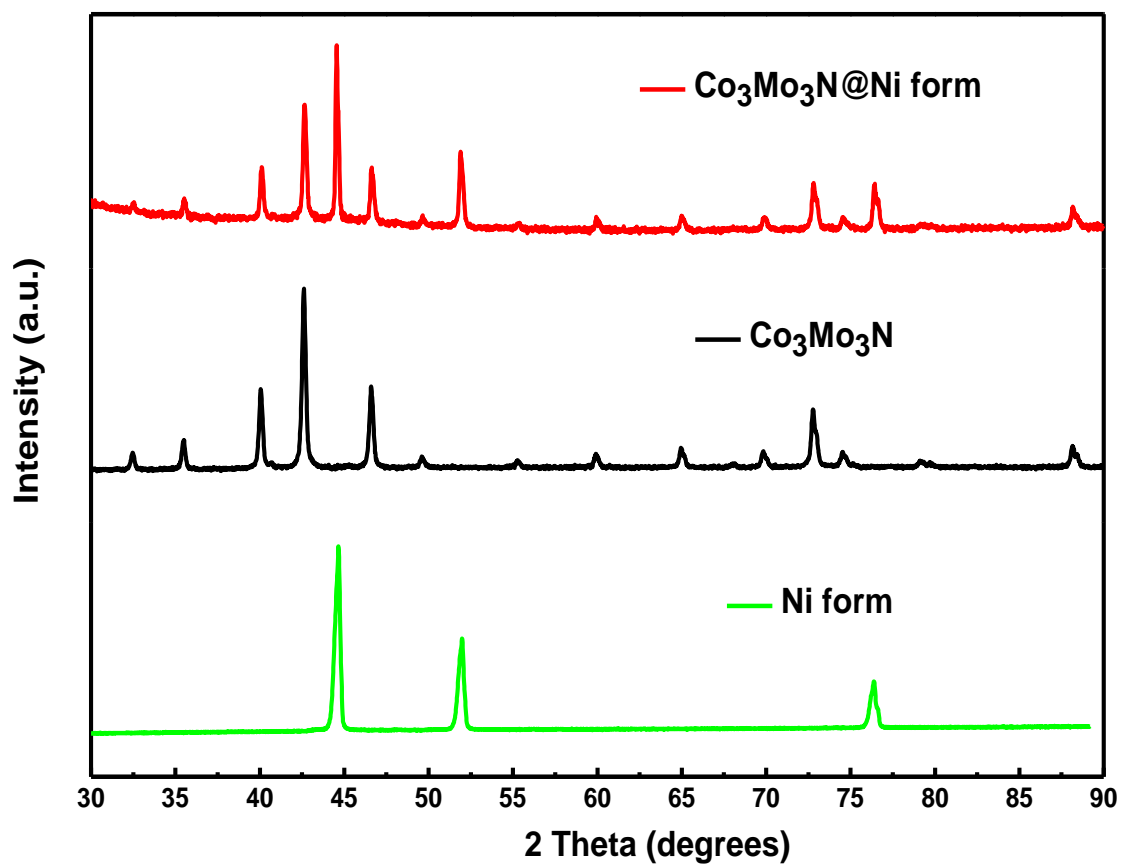


Figure S15. Powder X-ray diffraction patterns of Co₃Mo₃N composite on Ni foam prepared in H₂/N₂ mix at 750 °C (red); Co₃Mo₃N powder prepared in H₂/N₂ mix at 750 °C (black) and Ni foam (green).

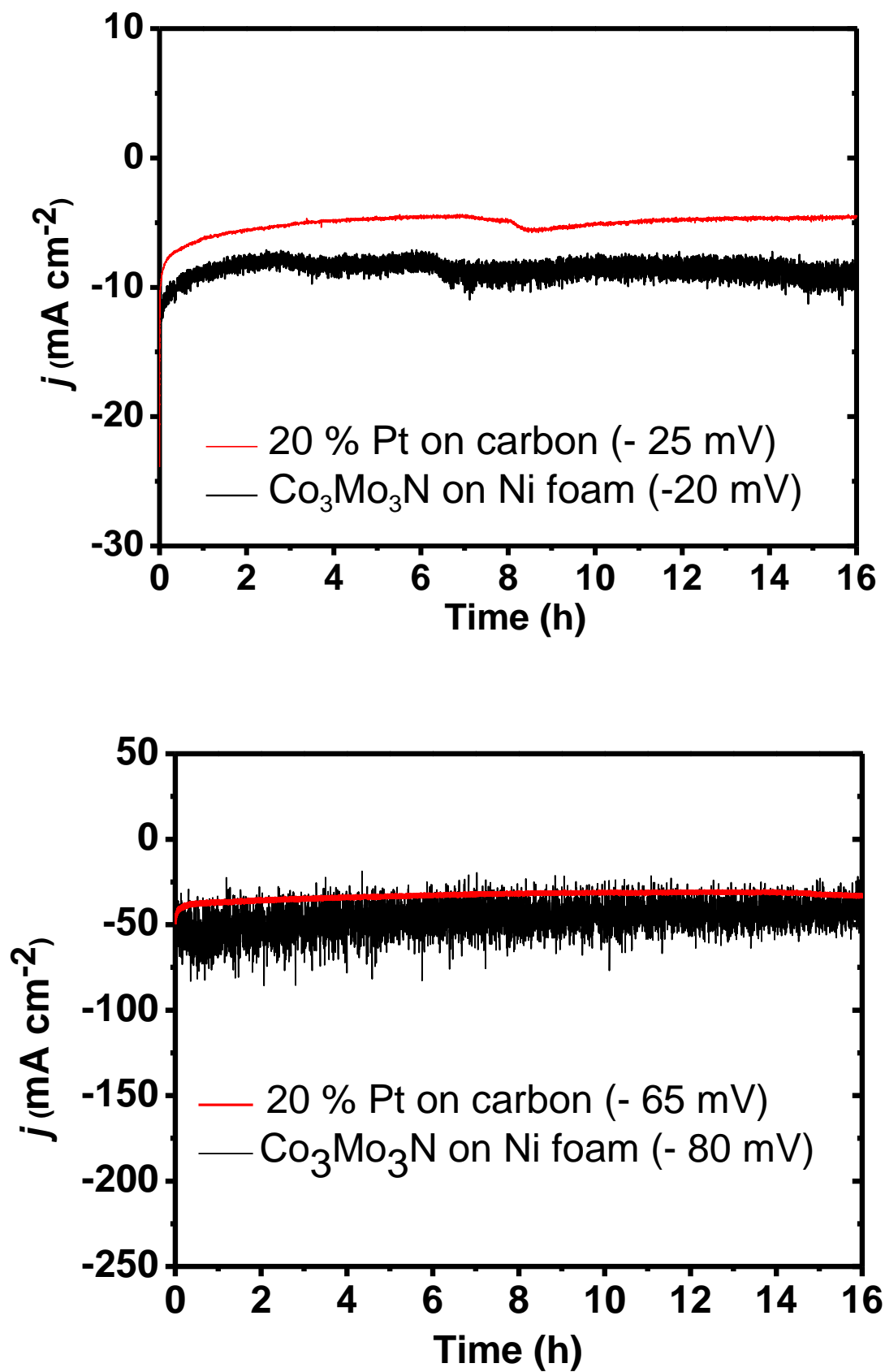


Figure S16. Chronoamperometry profiles of Co₃Mo₃N on Ni foam in comparison with electrode made from the commercial 20 % on carbon at applied potentials. The applied potentials are vs. RHE.

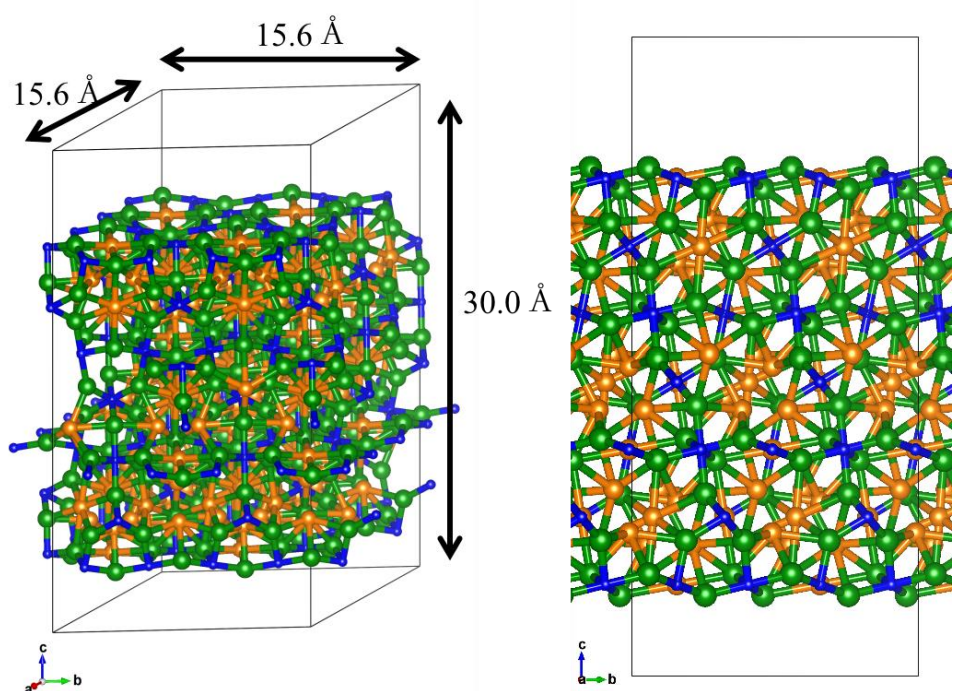


Figure S17. The 3D model of the 2×2 supercell (left) and the (111)-block (representative of both the $\text{Co}_3\text{Mo}_3\text{N}$ -(111) viewed along a -axis (right). Co, Mo and N are represented by orange, green and blue spheres.

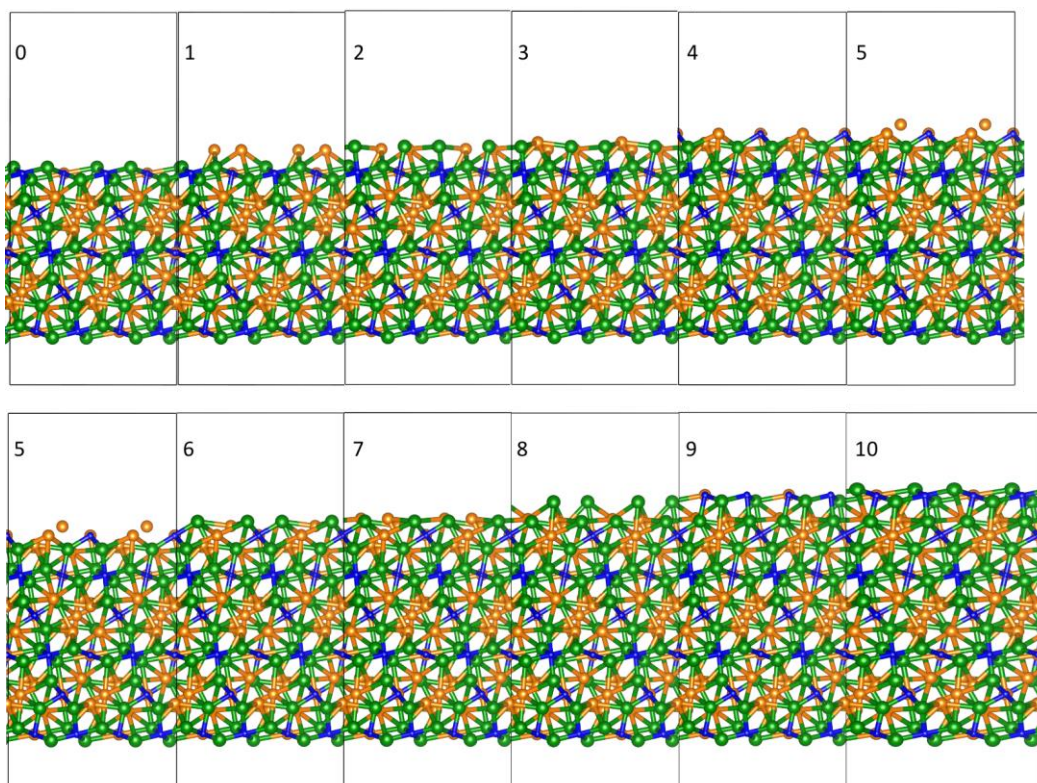


Figure S18. The ten possible $\text{Co}_3\text{Mo}_3\text{N}$ -(111) termination blocks viewed along a -axis. Co, Mo and N are represented by orange, green and blue spheres.

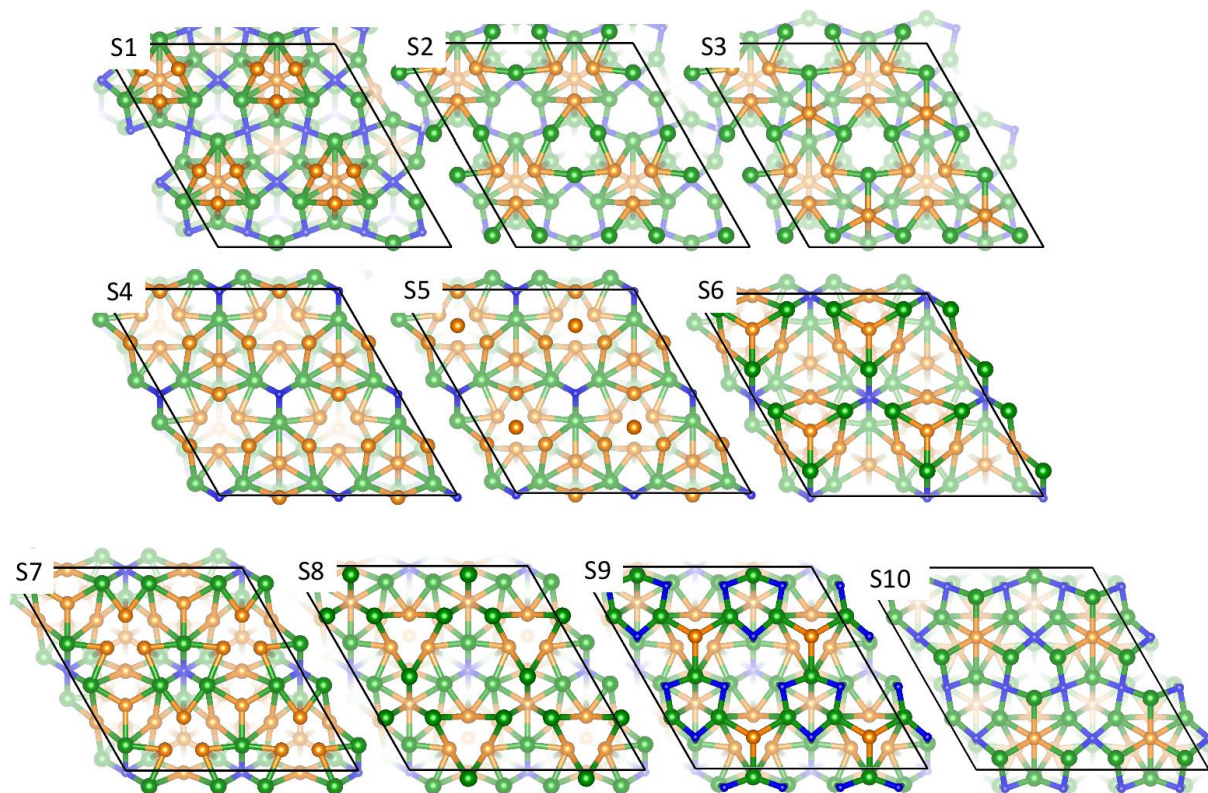


Figure S19. The ten possible 2×2 $\text{Co}_3\text{Mo}_3\text{N}$ -(111) surfaces displayed in Fig S12 viewed from top (along c -axis). Co, Mo and N are represented by orange, green and blue spheres. The surface S0 identified as the most stable is omitted as it is displayed in Figure 3a.

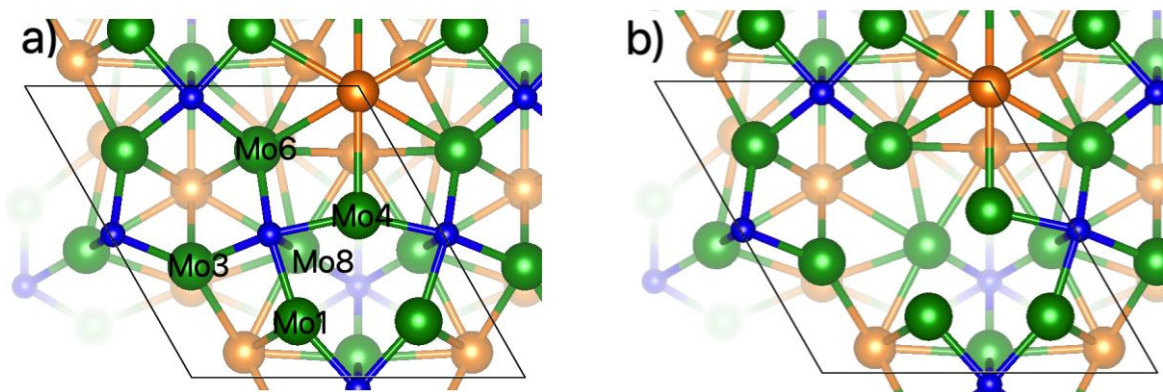


Figure S20. A magnified fragment of the original $\text{Co}_3\text{Mo}_3\text{N}$ -(111) corresponding to the most stable surface (a); the $\text{Co}_3\text{Mo}_3\text{N}$ -(111) with N-vacant site (b). Co, Mo and N are represented by orange, green and blue spheres.

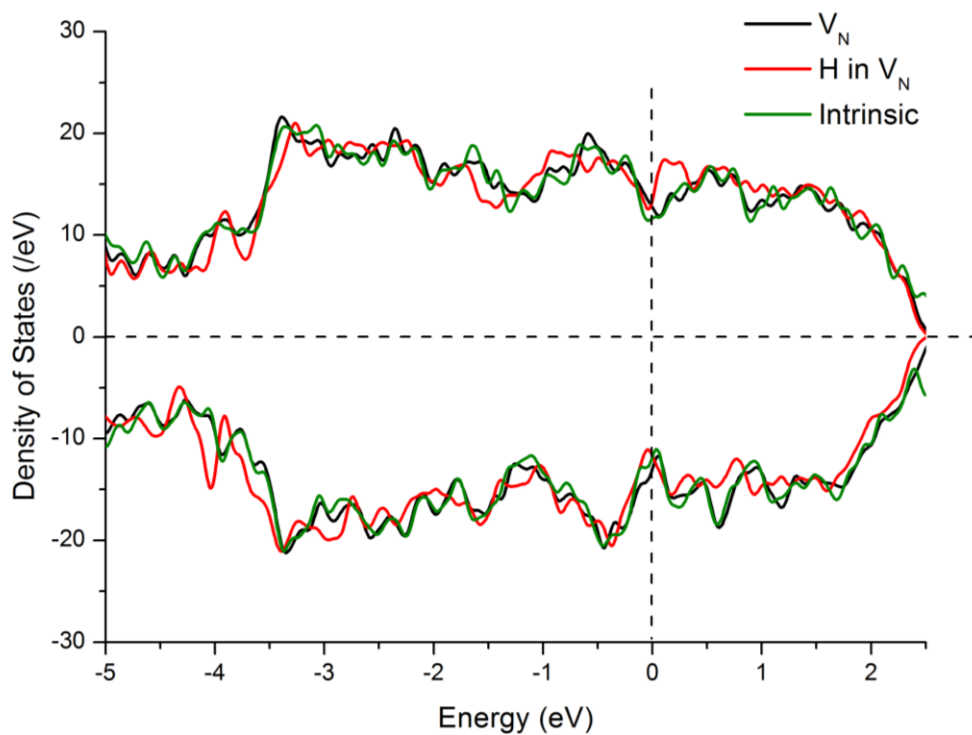


Figure S21. The total Density of States (DOS) of the intrinsic surface (green line), the surface with a N-vacancy (black line), and the surface that a H filled in the N-vacancy (red line).

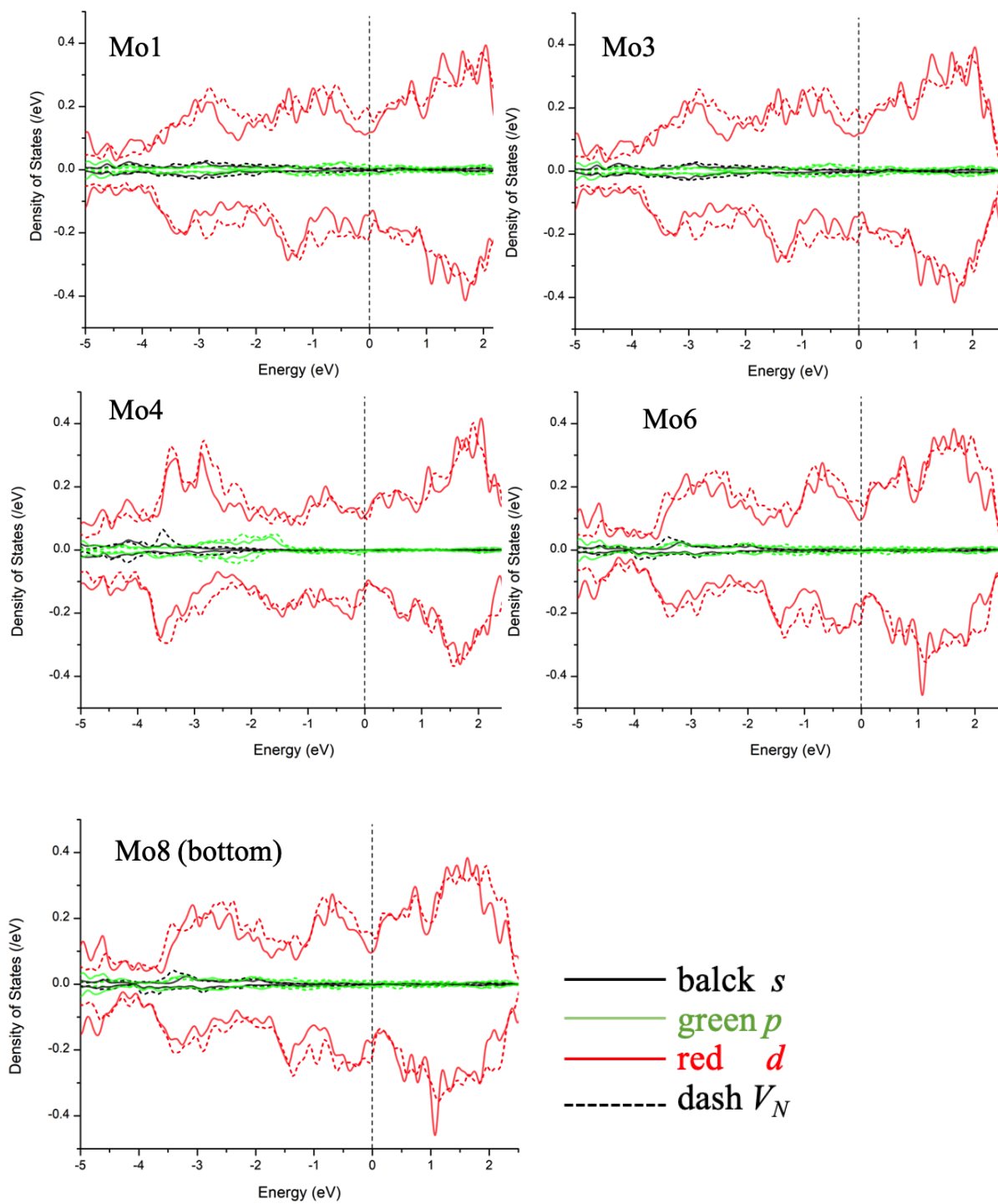


Figure S22. The partial PDOS of Mo atoms in proximity to the N-atom and N-vacancy in the intrinsic surface and the N-vacancy surface. The locations of atoms are shown in Figure S14.

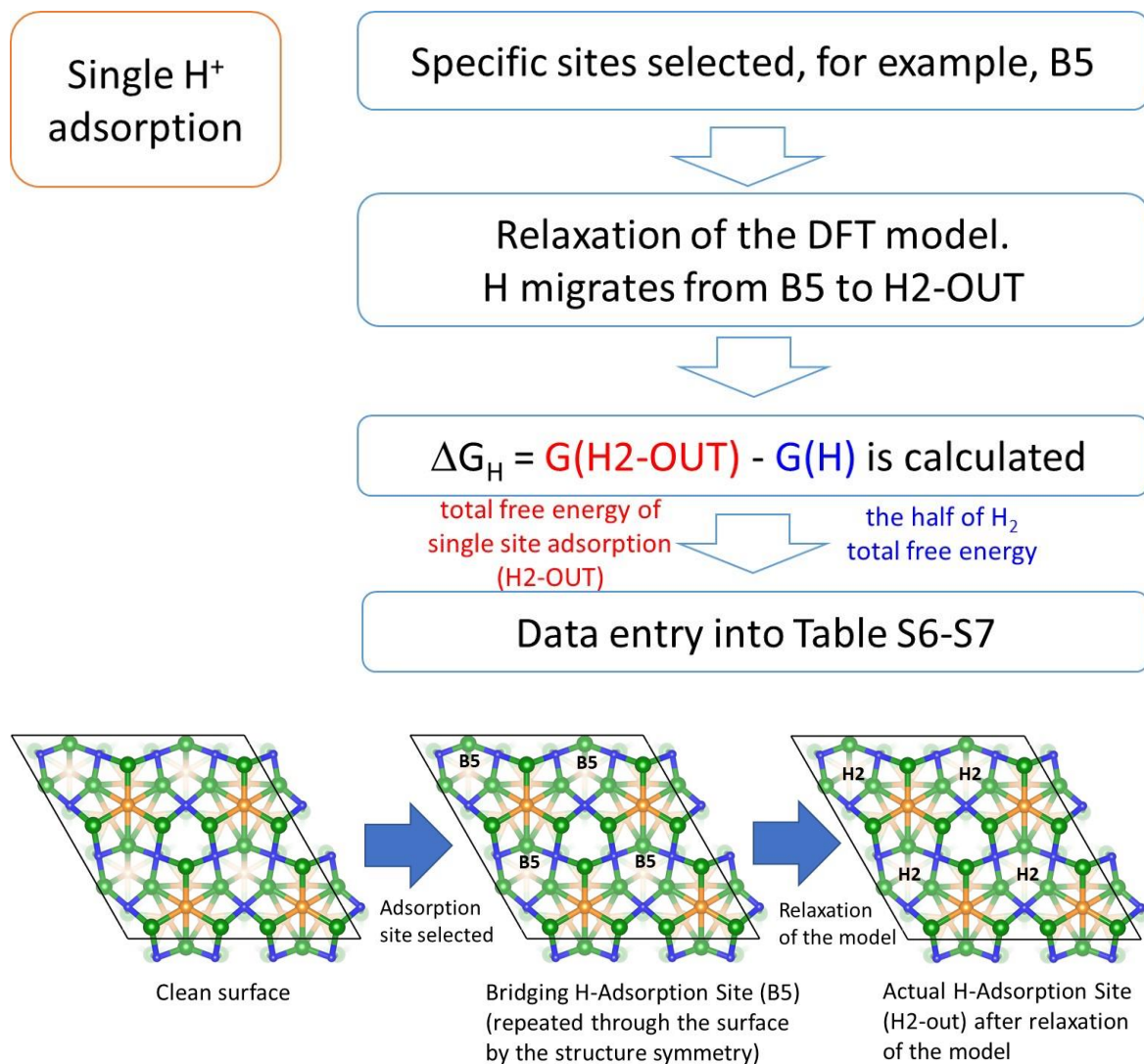


Figure S23. A schematic representation of the algorithm taken to calculate ΔG_{Hads} for a single site adsorption model.

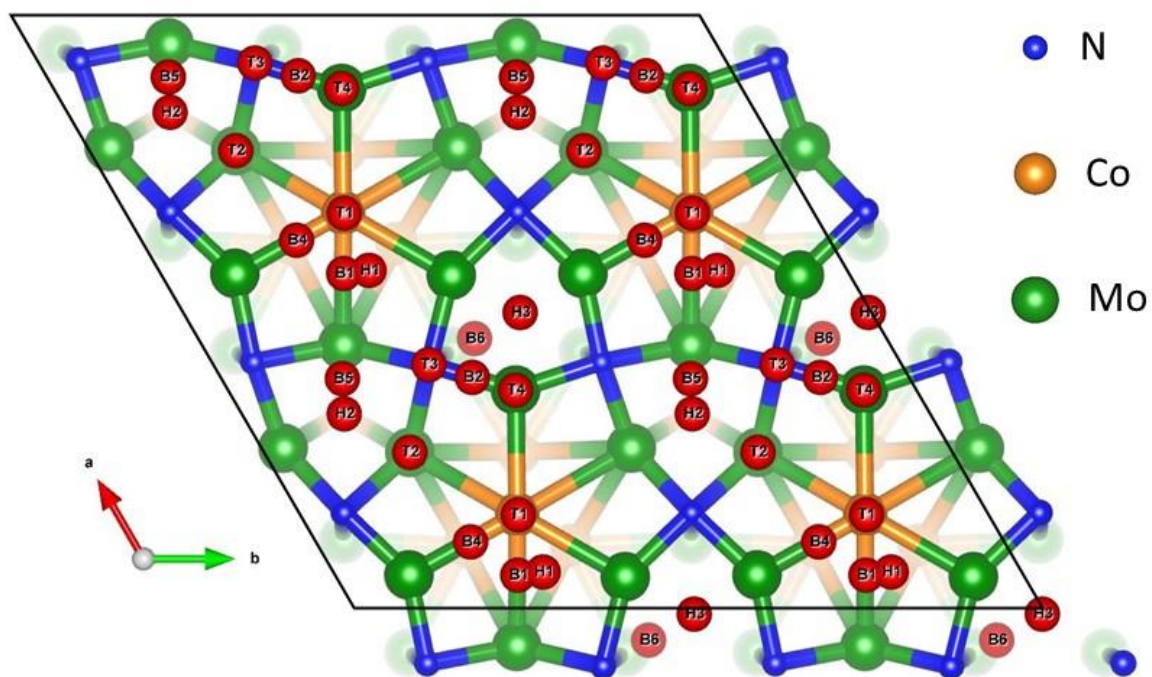


Figure S24. The location of ALL initially tested adsorption sites (red spheres) on 2×2 $\text{Co}_3\text{Mo}_3\text{N}$ -(111) surface. The energies of the sites are given in Table S6. It should be noted that only one site was used in each simulation for the single site model as outlined in the algorithm in Fig. S17.

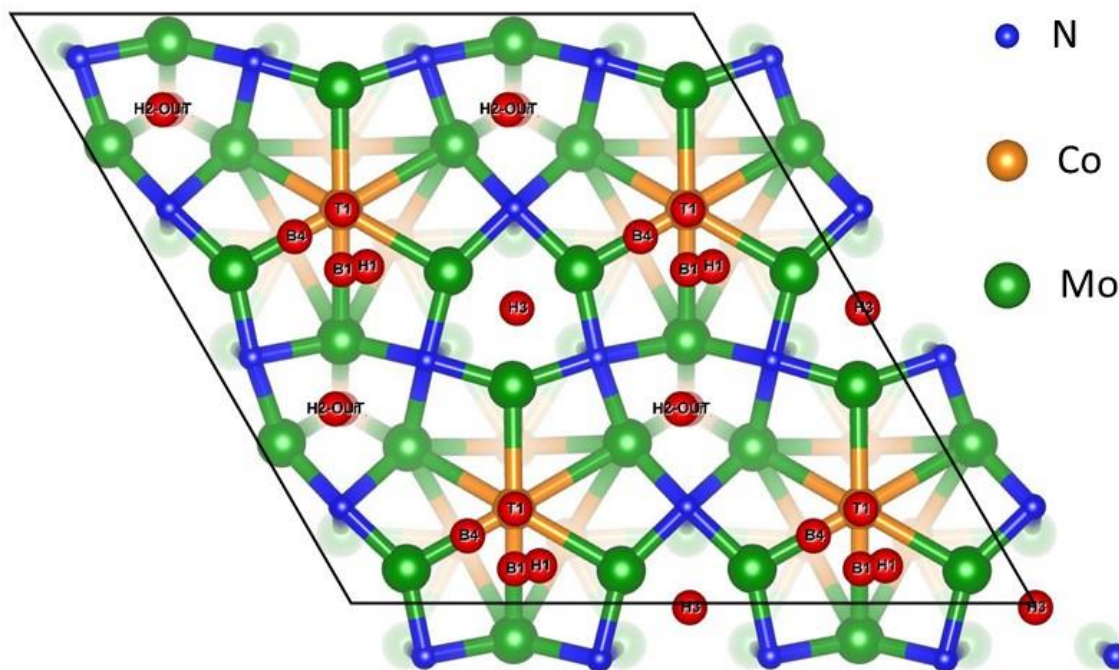


Figure S25. The location of ALL optimal adsorption sites (red spheres) on 2×2 $\text{Co}_3\text{Mo}_3\text{N}$ -(111) surface. The energies of the sites are given in Table S7. It should be noted that only one site was used in each simulation for the single site model as outlined in the algorithm in Fig. S17.

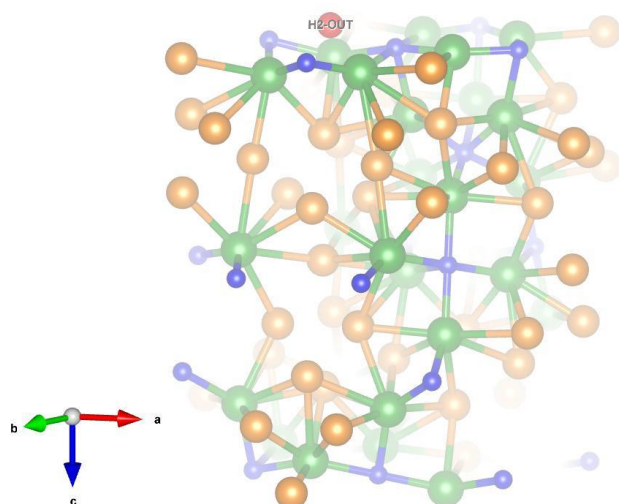


Figure S26. The location of the adsorbed hydrogen on the hollow H2-OUT site (red sphere) with respect to the most stable surface of $\text{Co}_3\text{Mo}_3\text{N}$ -(111) slab, using a representative 3D fragment. Co, Mo and N are represented by orange, green and blue spheres.

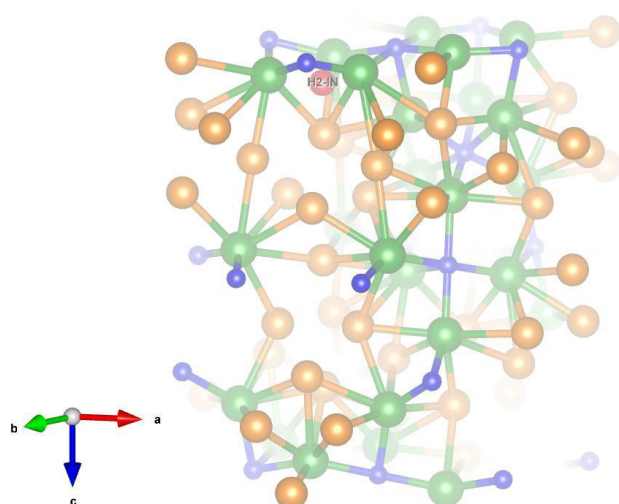


Figure S27. The location of the adsorbed hydrogen on the hollow H2-IN site (red sphere) with respect to the most stable surface of $\text{Co}_3\text{Mo}_3\text{N}$ -(111) slab, using a representative 3D fragment. Co, Mo and N are represented by orange, green and blue spheres.

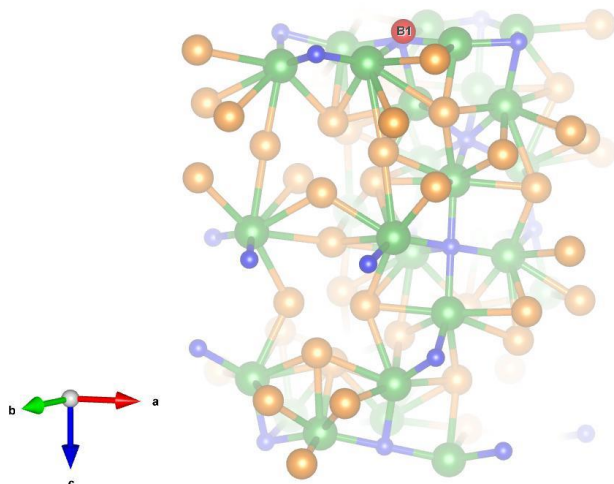


Figure S28. The location of the adsorbed hydrogen on the bridging B1 site (red sphere) with respect to the most stable surface of $\text{Co}_3\text{Mo}_3\text{N}$ -(111) slab, using a representative 3D fragment. Co, Mo and N are represented by orange, green and blue spheres.

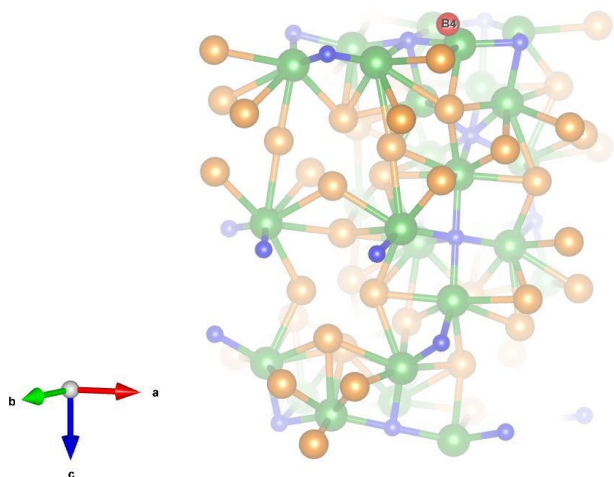


Figure S29. The location of the adsorbed hydrogen on the bridging B4 site (red sphere) with respect to the most stable surface of $\text{Co}_3\text{Mo}_3\text{N}$ -(111) slab, using a representative 3D fragment. Co, Mo and N are represented by orange, green and blue spheres.

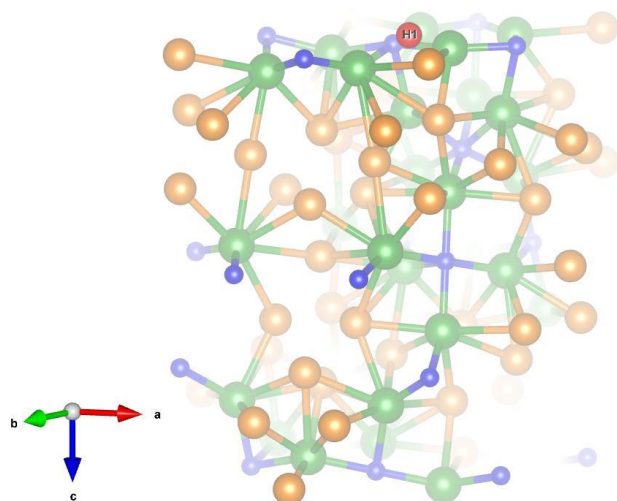


Figure S30. The location of the adsorbed hydrogen on the hollow H1 site (red sphere) with respect to the most stable surface of $\text{Co}_3\text{Mo}_3\text{N}$ -(111) slab, using a representative 3D fragment. Co, Mo and N are represented by orange, green and blue spheres.

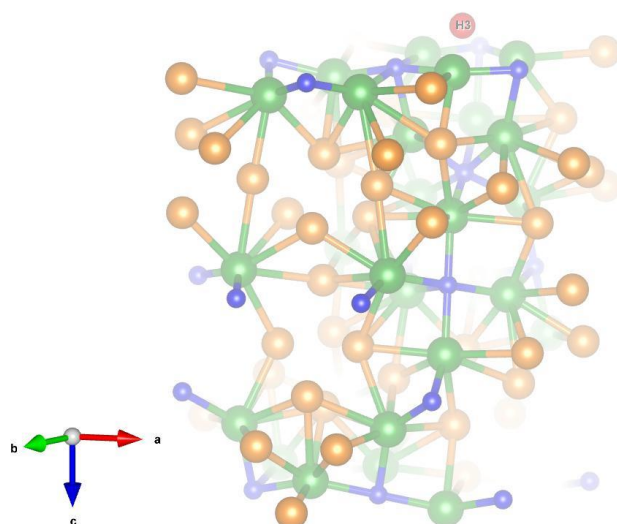


Figure S31. The location of the adsorbed hydrogen on the hollow H3 site (red sphere) with respect to the most stable surface of $\text{Co}_3\text{Mo}_3\text{N}$ -(111) slab, using a representative 3D fragment. Co, Mo and N are represented by orange, green and blue spheres.

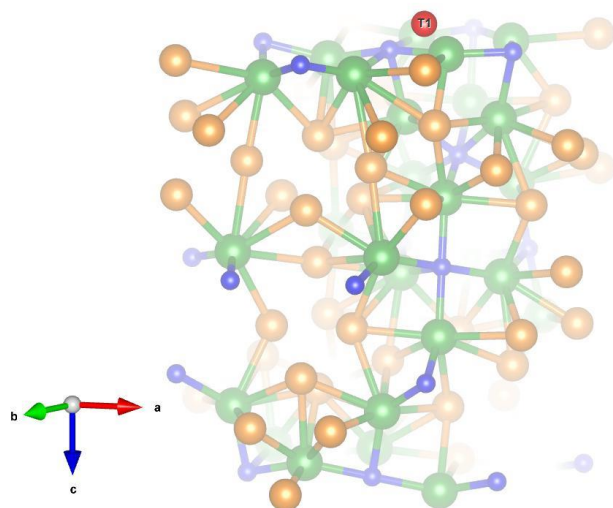


Figure S32. The location of the adsorbed hydrogen on the terminal T1 site (red sphere) with respect to the most stable surface of Co₃Mo₃N-(111) slab, using a representative 3D fragment. Co, Mo and N are represented by orange, green and blue spheres.

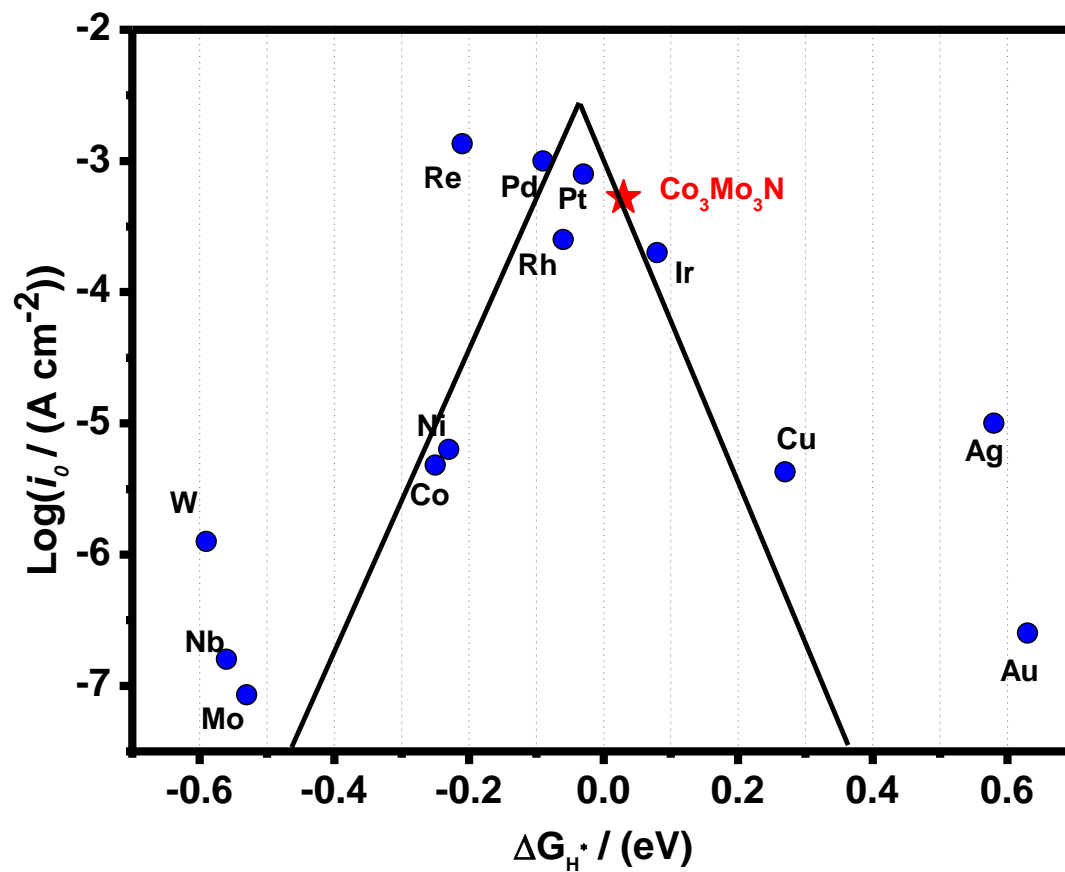


Figure S33. Volcano – plot built on the experimentally determined exchange current densities (values are taken from ref. 13) as a function of the calculated free energy for hydrogen adsorption.

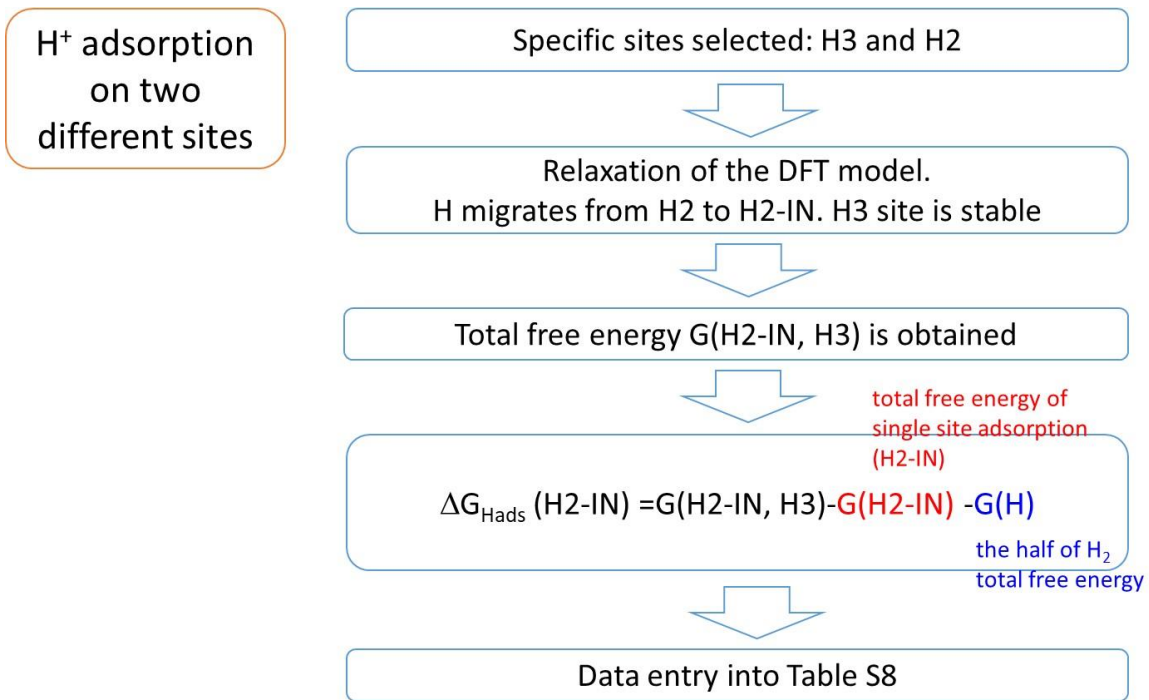


Figure S34. A schematic representation of the algorithm employed to calculate ΔG_{Hads} for a two site adsorption model.

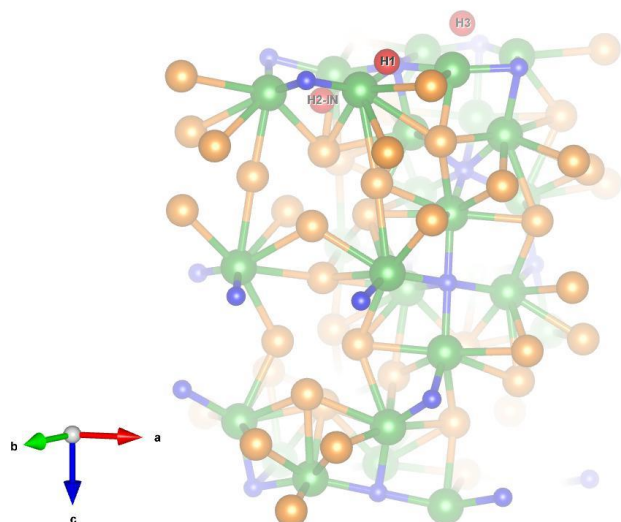


Figure S35. The location of the adsorbed hydrogen (red sphere) in the most stable configuration for simultaneous adsorption on three sites (H2-IN site acting as the reactive site) with respect to the most stable surface of Co₃Mo₃N-(111) slab, using a representative 3D fragment. Co, Mo and N are represented by orange, green and blue spheres.

References:

- (1) Bion, N.; Can, F.; Cook, J.; Hargreaves, J. S. J.; Hector, A. L.; Levason, W.; McFarlane, A. R.; Richard, M.; Sardar, K. The Role of Preparation Route upon the Ambient Pressure Ammonia Synthesis Activity of Ni₂Mo₃N. *Appl. Catal. A Gen.* **2015**, *504*, 44–50.
- (2) Conway, J. O.; Prior, T. J. Interstitial Nitrides Revisited – A Simple Synthesis of M_xMo₃N (M = Fe, Co, Ni). *J. Alloys Compd.* **2019**, *774*, 69–74.
- (3) Hunter, S. M.; McKay, D.; Smith, R. I.; Hargreaves, J. S. J.; Gregory, D. H. Topotactic Nitrogen Transfer: Structural Transformation in Cobalt Molybdenum Nitrides. *Chem. Mater.* **2010**, *22* (9), 2898–2907.
- (4) Chen, W. F.; Sasaki, K.; Ma, C.; Frenkel, A. I.; Marinkovic, N.; Muckerman, J. T.; Zhu, Y.; Adzic, R. R. Hydrogen-Evolution Catalysts Based on Non-Noble Metal Nickel-Molybdenum Nitride Nanosheets. *Angew. Chemie - Int. Ed.* **2012**, *51* (25), 6131–6135.
- (5) Cao, B.; Veith, G. M.; Neufeind, J. C.; Adzic, R. R.; Khalifah, P. G. Mixed Close-Packed Cobalt Molybdenum Nitrides as Non-Noble Metal Electrocatalysts for the Hydrogen Evolution Reaction. *J. Am. Chem. Soc.* **2013**, *135* (51), 19186–19192.
- (6) Jin, H.; Gu, Q.; Chen, B.; Tang, C.; Zheng, Y.; Zhang, H.; Jaroniec, M.; Qiao, S. Z. Molten Salt-Directed Catalytic Synthesis of 2D Layered Transition-Metal Nitrides for Efficient Hydrogen Evolution. *Chem* **2020**, *6* (9), 2382–2394.
- (7) Zhao, J.; Zeng, Y.; Wang, J.; Xu, Q.; Chen, R.; Ni, H.; Cheng, G. J. Ultrahigh Electrocatalytic Activity with Trace Amounts of Platinum Loadings on Free-Standing Mesoporous Titanium Nitride Nanotube Arrays for Hydrogen Evolution Reactions. *Nanoscale* **2020**, *12* (28), 15393–15401.
- (8) Wang, W.; Shao, Y.; Wang, Z.; Yang, Z.; Zhen, Z.; Zhang, Z.; Mao, C.; Guo, X.; Li, G. Synthesis of Ru-Doped VN by a Soft-Urea Pathway as an Efficient Catalyst for Hydrogen Evolution. *ChemElectroChem* **2020**, *7* (5), 1201–1206.
- (9) Liu, Z.; Zhang, X.; Song, H.; Yang, Y.; Zheng, Y.; Gao, B.; Fu, J.; Chu, P. K.; Huo, K. Electronic Modulation between Tungsten Nitride and Cobalt Dopants for Enhanced Hydrogen Evolution Reaction at a Wide Range of PH. *ChemCatChem* **2020**, *12* (11), 2962–2966.
- (10) Gu, Y.; Wu, A.; Jiao, Y.; Zheng, H.; Wang, X.; Xie, Y.; Wang, L.; Tian, C.; Fu, H. Two-Dimensional Porous Molybdenum Phosphide/Nitride Heterojunction Nanosheets for PH-

- Universal Hydrogen Evolution Reaction. *Angew. Chemie Int. Ed.* **2021**, *60* (12), 6673–6681.
- (11) Tan, J.; Mei, Y.; Shen, H.; Liu, H.; Azhagan, T.; Song, W.; Thomas, T.; Liu, J.; Yang, M.; Gao, M. Experimental and Theoretical Insights of MoS₂/Mo₃N₂ Nanoribbon-Electrocatalysts for Efficient Hydrogen Evolution Reaction. *ChemCatChem* **2020**, *12* (1), 122–128.
- (12) Jackson, S. K.; Layland, R. C.; Zur Loye, H. C. Simultaneous Powder X-Ray and Neutron Diffraction Refinement of Two η -Carbide Type Nitrides, Fe₃Mo₃N and Co₃Mo₃N, Prepared by Ammonolysis and by Plasma Nitridation of Oxide Precursors. *J. Alloys Compd.* **1999**, *291* (1–2), 94–101.
- (13) Prior, T. J.; Battle, P. D. Facile Synthesis of Interstitial Metal Nitrides with the Filled β -Manganese Structure. *J. Solid State Chem.* **2003**, *172* (1), 138–147.
- (14) Nørskov, J. K.; Bligaard, T.; Logadottir, A.; Kitchin, J. R.; Chen, J. G.; Pandelov, S.; Stimming, U. Trends in the Exchange Current for Hydrogen Evolution. *J. Electrochem. Soc.* **2005**, *152* (3), J23.